J|A|C|S
ARTICLES
Published on Web 02/20/2002

Framework Engineering by Anions and Porous Functionalities of Cu(II)/4,4′-bpy Coordination Polymers

Shin-ichiro Noro,[†] Ryo Kitaura,[†] Mitsuru Kondo,[†] Susumu Kitagawa,*[,†] Tomohiko Ishii,[‡] Hiroyuki Matsuzaka,[‡] and Masahiro Yamashita[‡]

Contribution from the Department of Synthetic Chemistry and Biological Chemistry, Graduate School of Engineering, Kyoto University, Yoshida, Sakyo-ku, Kyoto 606-8501, Japan, and Department of Chemistry, Graduate School of Science, Tokyo Metropolitan University, Minami-ohsawa, Hachioji-shi, Tokyo 192-0397, Japan

Received May 30, 2001

Abstract: A combination of framework-builder (Cu(II) ion and 4,4′-bipyridine (4,4′-bpy) ligand) and framework-regulator (AF_6 type anions; A = Si, Ge, and P) provides a series of novel porous coordination polymers. The highly porous coordination polymers $\{[Cu(AF_6)(4,4'\text{-bpy})_2]\cdot 8H_2O\}_n$ (A = Si (**1a**·$8H_2O$), Ge (**2a**·$8H_2O$)) afford robust 3-dimensional (3-D), microporous networks (*3-D Regular Grid*) by using AF_6^{2-} anions. The channel size of these complexes is ca. 8 × 8 Å^2 along the *c*-axis and 6 × 2 Å^2 along the *a*- or *b*-axes. When compounds **1a**·$8H_2O$ or **2a**·$8H_2O$ were immersed in water, a conversion of 3-D networks (**1a**·$8H_2O$ or **2a**·$8H_2O$) to interpenetrated networks $\{[Cu(4,4'\text{-bpy})_2(H_2O)_2]\cdot AF_6\}_n$ (A = Si (**1b**) and Ge (**2b**)) (*2-D Interpenetration*) took place. This 2-D interpenetrated network **1b** shows unique dynamic anion-exchange properties, which accompany drastic structural conversions. When a PF_6^- monoanion instead of AF_6^{2-} dianions was used as the framework-regulator with another co-counteranion (coexistent anions), porous coordination polymers with various types of frameworks, $\{[Cu_2(4,4'\text{-bpy})_5(H_2O)_4]\cdot\text{anions}\cdot 2H_2O\cdot 4EtOH\}_n$ (anions = $4PF_6^-$ (**3**·$2H_2O$·4EtOH), $2PF_6^- + 2ClO_4^-$ (**4**·$2H_2O$·4EtOH)) (*2-D Double-Layer*), $\{[Cu_2(PF_6)(NO_3)(4,4'\text{-bpy})_4]\cdot 2PF_6\cdot 2H_2O\}_n$ (**5**·$2PF_6$·$2H_2O$) (*3-D Undulated Grid*), $\{[Cu(PF_6)(4,4'\text{-bpy})_2(MeCN)]\cdot PF_6\cdot 2MeCN\}_n$ (**6**·2MeCN) (*2-D Grid*), and $\{[Cu(4,4'\text{-bpy})_2(H_2O)_2]\cdot PF_6\cdot BF_4\}_n$ (**7**) (*2-D Grid*), were obtained, where the three modes of PF_6^- anions are observed. **5**·$2PF_6$·$2H_2O$ has rare PF_6^- bridges. The PF_6^- and NO_3^- monoanions alternately link to the Cu(II) centers in the undulated 2-D sheets of $[Cu(4,4'\text{-bpy})_2]_n$ to form a 3-D porous network. The free PF_6^- anions are included in the channels. **6**·2MeCN affords both free and terminal-bridged PF_6^- anions. **3**·$2H_2O$·4EtOH, **4**·$2H_2O$·4EtOH, and **7** bear free PF_6^- anions. All of the anions in **3**·$2H_2O$·4EtOH and **4**·$2H_2O$·4EtOH are freely located in the channels constructed from a host network. Interestingly, these Cu(II) frameworks are rationally controlled by counteranions and selectively converted to other frameworks.

Introduction

The study of self-assembled coordination polymers containing transition metal ions and organic bridging ligands has been carried out by many researchers during the past decade.[1−10] Coordination polymers having flexible or rigid microporous channels are especially of great interest due to their unique properties such as physical gas adsorption,[11−26] chemical adsorption,[12,16,27−31] ion-exchange,[32−35] heterogeneous catalysis,[36−38] and so on. The porous coordination polymers have advantages in that they provide not only light materials with

* To whom correspondence should be addressed. Telephone: 81-75-753-5652. Fax: 81-75-753-4979. E-mail: kitagawa@sbchem.kyoto-u.ac.jp.
[†] Kyoto University.
[‡] Tokyo Metropolitan University.

(1) Yaghi, O. M. *Access Nanoporous Mater.* **1995**, 111−121.
(2) Yaghi, O. M.; Li, H.; Davis, C.; Richardson, D.; Groy, T. L. *Acc. Chem. Res.* **1998**, *31*, 474−484.
(3) Zaworotko, M. J. *Chem. Soc. Rev.* **1994**, 283−288.
(4) Zaworotko, M. J. *Chem. Commun.* **2001**, 1−9.
(5) Hagrman, P. J.; Hagrman, D.; Zubieta, J. *Angew. Chem., Int. Ed.* **1999**, *38*, 2638−2684.
(6) Janiak, C. *Angew. Chem., Int. Ed. Engl.* **1997**, *36*, 1431−1434.
(7) Kitagawa, S.; Kondo, M. *Bull. Chem. Soc. Jpn.* **1998**, *71*, 1739−1753.
(8) Blake, A. J.; Champness, N. R.; Hubberstey, P.; Li, W.-S.; Withersby, M. A.; Schröder, M. *Coord. Chem. Rev.* **1999**, *183*, 117−138.
(9) Eddaoudi, M.; Moler, D. B.; Li, H.; Chen, B.; Reineke, T. M.; O'Keeffe, M.; Yaghi, O. M. *Acc. Chem. Res.* **2001**, *34*, 319−330.
(10) Moulton, B.; Zaworotko, M. J. *Chem. Rev.* **2001**, *101*, 1629−1658.
(11) Yaghi, O. M.; Li, G.; Li, H. *Nature* **1995**, *378*, 703−706.
(12) Eddaoudi, M.; Li, H.; Yaghi, O. M. *J. Am. Chem. Soc.* **2000**, *122*, 1391−1397.
(13) Li, H.; Eddaoudi, M.; Groy, T. L.; Yaghi, O. M. *J. Am. Chem. Soc.* **1998**, *120*, 8571−8572.
(14) Li, H.; Eddaoudi, M.; O'Keeffe, M.; Yaghi, O. M. *Nature* **1999**, *402*, 276−279.
(15) Reineke, T. M.; Eddaoudi, M.; O'Keeffe, M.; Yaghi, O. M. *Angew. Chem., Int. Ed.* **1999**, *38*, 2590−2594.
(16) Chui, S. S.-Y.; Lo, S. M.-F.; Charmant, J. P. H.; Orpen, A. G.; Williams, I. D. *Science* **1999**, *283*, 1148−1150.
(17) Kondo, M.; Yoshitomi, T.; Seki, K.; Matsuzaka, H.; Kitagawa, S. *Angew. Chem., Int. Ed. Engl.* **1997**, *36*, 1725−1727.
(18) Kondo, M.; Okubo, T.; Asami, A.; Noro, S.; Yoshitomi, T.; Kitagawa, S.; Ishii, T.; Matsuzaka, H.; Seki, K. *Angew. Chem., Int. Ed.* **1999**, *38*, 140−143.
(19) Kondo, M.; Shimamura, M.; Noro, S.; Minakoshi, S.; Asami, A.; Seki, K.; Kitagawa, S. *Chem. Mater.* **2000**, *12*, 1288−1299.
(20) Noro, S.; Kitagawa, S.; Kondo, M.; Seki, K. *Angew. Chem., Int. Ed.* **2000**, *39*, 2082−2084.
(21) Mori, W.; Inoue, F.; Yoshida, K.; Nakayama, H.; Takamizawa, S.; Kishita, M. *Chem. Lett.* **1997**, 1219−1220.

10.1021/ja0113192 CCC: $22.00

high porosity but also desirable regular networks. Werner complexes,[39] Prussian blue compounds,[40−42] and Hofmann clathrates and their derivatives[43] are widely known as porous materials that can reversibly adsorb small molecules. There are also numerous examples of porous organic frameworks that are sustained by hydrogen bonds.[44−49] Previously, we have defined the porous compounds in the three categories.[7] The first generation compounds afford microporous channels with guest molecules, which are destroyed by the removal of all guest molecules. The second generation compounds have rigid vacant channels formed after the removal of guest molecules. The third generation compounds bear flexible channels, which change their own frameworks responding to an external physical stimulus, such as pressure and light, and a chemical stimulus by guest molecules. A large number of dicarboxylate- or tricarboxylate-bridged porous coordination polymers have been hitherto synthesized, and their porous functions have been investigated.[11−15,24,25,29−31,50] These carboxylate-bridged porous coordination polymers tend to provide a rigid framework because of the two site-binding modes of anionic carboxylate groups, therefore classified as the second generation compounds. Recently, several coordination polymers have been prepared, where these frameworks change reversibly on removal/clathration of guest molecules or anions.[31,50−55] The porous coordination polymers of 4,4′-bpy have relatively flexible frameworks based on the single site-binding of neutral pyridyl groups, potentially affording the third generation compounds evolving from those of the second generation .[17,20,33,36] On this background, we have been challenged to develop a new type of coordination polymer chemistry of 4,4′-bpy. Recent synthetic chemistry of coordination polymers has so far been mainly focused on transition metal ions and coligands. This is because framework is due to the topology and geometry of both ligands and metal cations. In this sense, a pair of a metal and a ligand is regarded as a framework-builder. In addition, we noted counteranions, which have not only a role to neutralize overall charge in the solid but also to regulate frameworks; therefore we called this anion a framework-regulator. As shown in Scheme 1, AF_6^{2-} (A = Si, Ge) and PF_6^- anions are utilized, resulting in a key for construction, interconversion, and restoration of frameworks.

Scheme 1

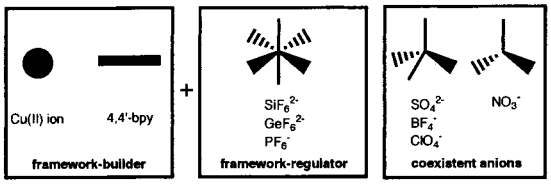

Cu(II) complexes could be relevant for crystal engineering by framework-builder/-regulator, liable to undergo the Jahn−Teller effect, resulting in a (4 + 2) coordination. In the presence of the 4,4′-bpy ligand, the AF_6 anions tend to sit at the axial sites of the Cu(II) ion. By utilizing this tendency, the control of the framework by anions could be carried out. Moreover, we introduced additional coexistent anions such as NO_3^-, BF_4^-, ClO_4^-, and SO_4^{2-} (Scheme 1), which afford various shapes (tetrahedral or trigonal), sizes, charges (mono- or dianion), and coordinate atoms (O or F) in the PF_6^- system to closely study the influence of the counteranion in the Cu/4,4′-bpy system.

In this paper, we obtained the following porous coordination polymers, $\{[Cu(AF_6)(4,4'\text{-bpy})_2]\cdot 8H_2O\}_n$ (A = Si (**1a**·$8H_2O$), Ge (**2a**·$8H_2O$)) (*3-D Regular Grid*), $\{[Cu(4,4'\text{-bpy})_2(H_2O)_2]\cdot AF_6\}_n$ (A = Si (**1b**), Ge (**2b**)) (*2-D Interpenetration*), $\{[Cu_2(4,4'\text{-bpy})_5(H_2O)_4]\cdot anions\cdot 2H_2O\cdot 4EtOH\}_n$ (anions = $4PF_6^-$ (**3**·$2H_2O$·4EtOH), $2PF_6^- + 2ClO_4^-$ (**4**·$2H_2O$·4EtOH)) (*2-D Double-Layer*), $\{[Cu_2(PF_6)(NO_3)(4,4'\text{-bpy})_4]\cdot 2PF_6\cdot 2H_2O\}_n$ (**5**·$2PF_6$·$2H_2O$) (*3-D Undulated Grid*), $\{[Cu(PF_6)(4,4'\text{-bpy})_2(MeCN)]\cdot PF_6\cdot 2MeCN\}_n$ (**6**·2MeCN) (*2-D Grid*), and $\{[Cu(4,4'\text{-bpy})_2(H_2O)_2]\cdot PF_6\cdot BF_4\}_n$ (**7**) (*2-D Grid*), which were crystallographically characterized, and their porous functions were investigated. In these complexes, 3-D networks (**1a**·$8H_2O$, **2a**·$8H_2O$, and **5**·$2PF_6$·$2H_2O$) are the second generation compounds. A conversion of 3-D networks (**1a**·$8H_2O$ or **2a**·$8H_2O$) to interpenetrated networks (**1b** and **2b**) took place while being immersed in water. Compound **1b** shows unprecedented dynamic anion-exchange properties and is classified as the third generation compound. When the PF_6^- anion was used together with coexistent anions in the reaction with the Cu(II) ion and 4,4′-bpy, various types of porous networks were constructed as shown in Scheme 2. In these PF_6^- complexes, only **5**·$2PF_6$·$2H_2O$ affords a 3-D porous

(22) Nukada, R.; Mori, W.; Takamizawa, S.; Mikuriya, M.; Handa, M.; Naono, H. *Chem. Lett.* **1999**, 367−368.
(23) Takamizawa, S.; Mori, W.; Furihata, M.; Takeda, S.; Yamaguchi, K. *Inorg. Chim. Acta* **1998**, *283*, 268−274.
(24) Seki, K.; Takamizawa, S.; Mori, W. *Chem. Lett.* **2001**, 122−123.
(25) Seki, K.; Takamizawa, S.; Mori, W. *Chem. Lett.* **2001**, 332−333.
(26) Li, D.; Kaneko, K. *Chem. Phys. Lett.* **2001**, *335*, 50−56.
(27) Yaghi, O. M.; Li, H.; Groy, T. L. *J. Am. Chem. Soc.* **1996**, *118*, 9096−9101.
(28) Yaghi, O. M.; Davis, C. E.; Li, G.; Li, H. *J. Am. Chem. Soc.* **1997**, *119*, 2861−2868.
(29) Li, H.; Davis, C. E.; Groy, T. L.; Kelley, D. G.; Yaghi, O. M. *J. Am. Chem. Soc.* **1998**, *120*, 2186−2187.
(30) Reineke, T. M.; Eddaoudi, M.; Fehr, M.; Kelley, D.; Yaghi, O. M. *J. Am. Chem. Soc.* **1999**, *121*, 1651−1657.
(31) Choi, H. J.; Lee, T. S.; Suh, M. P. *Angew. Chem., Int. Ed.* **1999**, *38*, 1405−1408.
(32) Yaghi, O. M.; Li, H. *J. Am. Chem. Soc.* **1995**, *117*, 10401−10402.
(33) Yaghi, O. M.; Li, H. *J. Am. Chem. Soc.* **1996**, *118*, 295−296.
(34) Yaghi, O. M.; Li, H.; Groy, T. L. *Inorg. Chem.* **1997**, *36*, 4292−4293.
(35) Hoskins, B. F.; Robson, R. *J. Am. Chem. Soc.* **1990**, *112*, 1546−1554.
(36) Fujita, M.; Kwon, Y. J.; Washizu, S.; Ogura, K. *J. Am. Chem. Soc.* **1994**, *116*, 1151−1152.
(37) Sawaki, T.; Dewa, T.; Aoyama, Y. *J. Am. Chem. Soc.* **1998**, *120*, 8539−8640.
(38) Seo, J. S.; Whang, D.; Lee, H.; Jun, S. I.; Oh, J.; Jeon, Y. J.; Kim, K. *Nature* **2000**, *404*, 982−986.
(39) Barrer, R. M. In *Molecular Sieves*; Meier, W. M., Utyyerhoeven, J. B., Eds.; ACS Advances in Chemistry Series 121; American Chemical Society: Washington, DC, 1974; p 1.
(40) Wilde, R. E.; Ghosh, S. N.; Marshall, B. J. *Inorg. Chem.* **1970**, *9*, 2512−2516.
(41) Buser, H. J.; Schwarzenbach, D.; Petter, W.; Ludi, A. *Inorg. Chem.* **1977**, *16*, 2704−2710.
(42) Dunbar, K. R.; Heintz, R. A. *Prog. Inorg. Chem.* **1997**, *45*, 283−391.
(43) Iwamoto, T. In *Inclusion Compounds*; Atwood, J. L., Davies, J. E. D., MacNicol, D. D., Eds.; Oxford: New York, 1991; Vol. 5, p 177.
(44) Endo, K.; Sawaki, T.; Koyanagi, M.; Kobayashi, K.; Masuda, H.; Aoyama, Y. *J. Am. Chem. Soc.* **1995**, *117*, 8341−8352.
(45) Endo, K.; Koike, T.; Sawaki, T.; Hyashida, O.; Masuda, H.; Aoyama, Y. *J. Am. Chem. Soc.* **1997**, *119*, 4117−4122.
(46) Dewa, T.; Endo, K.; Aoyama, Y. *J. Am. Chem. Soc.* **1998**, *120*, 8933−8940.
(47) Dewa, T.; Aoyama, Y. *Chem. Lett.* **2000**, 854−855.
(48) Dewa, T.; Saiki, T.; Imai, Y.; Endo, K.; Aoyama, Y. *Bull. Chem. Soc. Jpn.* **2000**, *73*, 2123−2127.
(49) Tanaka, T.; Endo, K.; Aoyama, Y. *Chem. Lett.* **2000**, 1424−1425.
(50) Kepert, C. J.; Prior, T. J.; Rosseinsky, M. J. *J. Am. Chem. Soc.* **2000**, *122*, 5158−5168.
(51) Soldatov, D. V.; Ripmeester, J. A.; Shergina, S. I.; Sokolov, I. E.; Zanina, A. S.; Gromilov, S. A.; Dyadin, Y. A. *J. Am. Chem. Soc.* **1999**, *121*, 4179−4188.
(52) Min, K. S.; Suh, M. P. *J. Am. Chem. Soc.* **2000**, *122*, 6834−6840.
(53) Min, K. S.; Suh, M. P. *Chem.-Eur. J.* **2001**, *7*, 303−313.
(54) Tabares, L. C.; Navarro, J. A. R.; Salas, J. M. *J. Am. Chem. Soc.* **2001**, *123*, 383−387.
(55) Jung, O.-S.; Kim, Y. J.; Lee, Y.-A.; Park, J. K.; Chae, H. K. *J. Am. Chem. Soc.* **2000**, *122*, 9921−9925.

Scheme 2

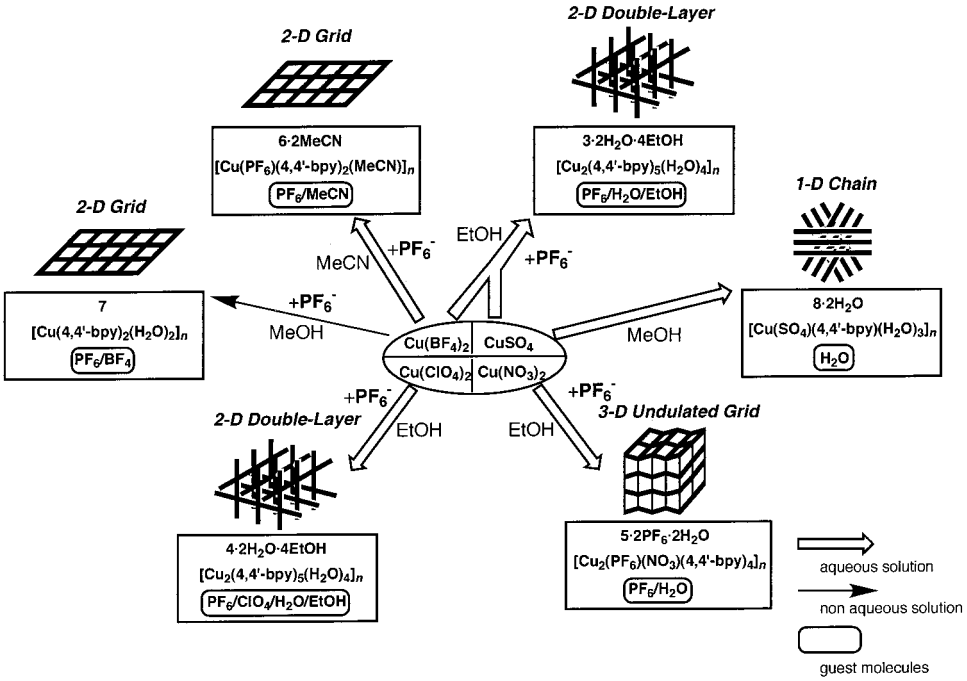

framework, in which 2-D undulated layers of $[Cu(4,4'\text{-bpy})_2]_n$ are bridged by PF_6^- and NO_3^- anions alternately. Other coordination polymers (**3**·$2H_2O$·4EtOH, **4**·$2H_2O$·4EtOH, **6**·2MeCN, and **7**) represent 2-D porous networks, but their detailed structures are clearly different from each other. This observation of the coexistent effect of counteranions is the first example.

Experimental Section

Physical Measurements. Elemental analyses were taken on Yanaco C,H,N Corder MT-5. IR spectra were recorded on a Hitachi I-5040FT-IR spectrometer with samples prepared as KBr pellets. UV−vis reflection spectra were recorded on a Hitachi U-3500 spectrophotometer over the range from 200 to 2700 nm at room temperature. X-ray powder diffraction (XRPD) data were collected on a MAC Science Instruments M21X-SRA by using Cu Kα radiation. Thermal gravimetric analyses (TGA) were carried out with a Rigaku Instruments TG8120 in a nitrogen atmosphere (heating rate: 5 K/min).

Gas Adsorption Measurements. The adsorption isotherms of methane gas on the sample were measured using a Cahn R-100 electrobalance and according to an already published procedure.[17] The adsorption isotherms of argon gas were measured using ASAP 2000M volumetric adsorption equipment from Micromeritics, Norcross, GA. The adsorption isotherms of nitrogen gas were measured using BELSORP28 volumetric adsorption equipment from Bel Japan, Inc.

Zeolite 5A was purchased from Bayer Co. The adsorption isotherms of methane gas were measured with the same method as for the sample. The adsorption properties of zeolites have been reported by L. Mentasty et al.,[56] and the methane adsorption quantity (2.9 mmol g^{-1} at 36 atm) of zeolite 5A was smaller than that of our experimental data (3.7 mmol g^{-1} at 36 atm). Therefore, we used the higher methane adsorption quantity as comparison data with the sample.

X-ray Structure Determination. A single crystal for each compound was mounted on a glass fiber and coated with epoxy resin. For **1b**, **3**·$2H_2O$·4EtOH, and **4**·$2H_2O$·4EtOH, X-ray data collections were carried out by a Rigaku Mercury diffractometer with graphite monochromated Mo Kα radiation. For **5**·$2PF_6$·$2H_2O$, **6**·2MeCN, and **10**·$5H_2O$, all measurements were made on a Rigaku RAXIS-RAPID imaging plate diffractometer with graphite monochromated Mo Kα radiation. For **2a**·$8H_2O$ and **2b**, all measurements were made on a Rigaku RAXIS-CS imaging plate diffractometer with graphite monochromated Mo Kα radiation. For **2a**·$8H_2O$, **2b**, and **3**-**6**, structures were solved by a direct method using the SIR92 program[57] and expanded using Fourier techniques.[58] For **1b**, the structure was solved by a direct method using the MITHRIL90 program[59] and expanded using Fourier techniques.[58] For **10**·$5H_2O$, the structure was solved by a direct method using the SHELXS-97 program[60] and expanded using Fourier techniques.[58] In all complexes, except **3**·$2H_2O$·4EtOH, the non-hydrogen atoms were refined anisotropically. In **3**·$2H_2O$·4EtOH, two carbon and one oxygen atoms of one EtOH molecule were fixed. All hydrogen atoms, which were placed in idealized positions, were included but not refined. The refinements were carried out using full-matrix least-squares techniques. Crystal data and details of the structure determinations are summarized in Table 1. Unfortunately, we could not obtain single crystals with a good quality for compounds **3**·$2H_2O$·4EtOH and **4**·$2H_2O$·4EtOH, and the data of the X-ray analysis were poorer than others. All calculations were performed using the teXsan[61] crystallographic software package of the Molecular Structure Corp.

Materials. $CuSO_4$·$5H_2O$, $Cu(NO_3)_2$·$3H_2O$, NH_4PF_6, and $(NH_4)_2SO_4$ were obtained from Wako Co. 4,4′-Bpy was purchased from Tokyo Kasei Industrial Co. $Cu(BF_4)_2$·xH_2O, $(NH_4)_2SiF_6$, and $(NH_4)_2GeF_6$ were obtained from Aldrich Chemical Co. $Cu(ClO_4)_2$·$6H_2O$ was obtained from Kanto Chemical Co.

Syntheses of {[Cu(SiF$_6$)(4,4′-bpy)$_2$]·8H$_2$O}$_n$ (1a·8H$_2$O) and {[Cu(4,4′-bpy)$_2$(H$_2$O)$_2$]·SiF$_6$}$_n$ (1b). The compound of **1a**·$8H_2O$ was synthesized as follows. A hot aqueous solution (20 mL) of $Cu(BF_4)_2$·xH_2O (266 mg, 1.12 mmol) and $(NH_4)_2SiF_6$ (199 mg, 1.12 mmol) was added to a hot ethylene glycol solution (40 mL) of 4,4′-bpy (350 mg,

(56) Mentasty, L.; Woestyn, A. M.; Zgrablich, G. *Adsorpt. Sci. Technol.* **1994**, *11*, 123−133.

(57) Altomare, A.; Burla, M. C.; Camalli, M.; Cascarano, M.; Giacovazzo, C.; Guagliardi, A.; Polidori, G. *J. Appl. Crystallogr.* **1994**, *27*, 435.

(58) Beurskens, P. T.; Admiraal, G.; Beurskens, G.; Bosman, W. P.; de Gelder, R.; Israel, R.; Smits, J. M. M. *The DIRDIF-94 Program System*; Technical Report of the Crystallography Laboratory; University of Nijmegen: The Netherlands, 1994.

(59) Gilmore, C. J. *MITHRIL − An Integrated Direct Methods Computer Program*; University of Glasgow: Scotland, 1990.

(60) Sheldrick, G. M. *Program for the Solution of Crystal Structures*; University of Goettingen: Germany, 1997.

(61) Crystal Structure Analysis Package, Molecular Structure Corporation (1985 & 1999).

Table 1. Crystallographic Data for $\{[Cu(4,4'\text{-bpy})_2(H_2O)_2]\cdot SiF_6\}_n$ (**1b**), $\{[Cu(GeF_6)(4,4'\text{-bpy})_2]\cdot 8H_2O\}_n$ (**2a**·$8H_2O$), $\{[Cu(4,4'\text{-bpy})_2(H_2O)_2]\cdot GeF_6\}_n$ (**2b**), $\{[Cu_2(4,4'\text{-bpy})_5(H_2O)_4]\cdot 4PF_6\cdot 2H_2O\cdot 4EtOH\}_n$ (**3**·$2H_2O$·4EtOH), $\{[Cu_2(4,4'\text{-bpy})_5(H_2O)_4]\cdot 2PF_6\cdot 2ClO_4\cdot 2H_2O\cdot 4EtOH\}_n$ (**4**·$2H_2O$·4EtOH), $\{[Cu_2(PF_6)(NO_3)(4,4'\text{-bpy})_4]\cdot 2PF_6\cdot 2H_2O\}_n$ (**5**·$2PF_6$·$2H_2O$), and $\{[Cu(PF_6)(4,4'\text{-bpy})_2(MeCN)]\cdot PF_6\cdot 2MeCN\}_n$ (**6**·2MeCN)

compounds	**1b**	**2a**·$8H_2O$	**2b**	**3**·$2H_2O$·4EtOH	**4**·$2H_2O$·4EtOH	**5**·$2PF_6$·$2H_2O$	**6**·2MeCN
formula	$C_{20}H_{20}N_4CuF_6O_2Si$	$C_{20}H_{32}N_4CuF_6GeO_8$	$C_{20}H_{20}N_4CuF_6GeO_2$	$C_{29}H_{38}N_5CuF_{12}O_5P_2$	$C_{29}H_{38}N_5CuClF_6O_9P$	$C_{40}H_{36}N_9Cu_2F_{18}O_5P_3$	$C_{26}H_{25}N_7CuF_{12}P_2$
fw	554.03	706.62	598.53	890.12	844.61	1284.77	789.00
crystal system	tetragonal	tetragonal	tetragonal	orthorhombic	orthorhombic	monoclinic	monoclinic
a, Å	11.080(2)	11.0934(5)	11.1835(6)	45.47(1)	44.870(10)	22.184(2)	11.1611(6)
b, Å				20.523(8)	20.292(5)	15.313(1)	13.1786(7)
c, Å	16.0239(7)	8.2070(6)	15.876(2)	8.229(3)	8.170(2)	11.1085(8)	22.1972(2)
β, deg						93.704(3)	92.569(3)
V, Å^3	1967.3(5)	1009.99(9)	1985.6(3)	7679(4)	7439(3)	3765.7(5)	3261.7(2)
space group	*P*4/*ncc* (No. 130)	*P*4/*mmm* (No. 123)	*P*4/*ncc* (No. 130)	*Aba*2 (No. 41)	*Aba*2 (No. 41)	*C*2/*m* (No. 12)	$P2_1/c$ (No. 14)
Z	4	1	4	8	8	2	4
ρ(calcd), g cm^{-3}	1.870	1.162	2.002	1.540	1.508	1.133	1.607
F(000)	1124.00	359.00	1196.00	3632.00	3472.00	1288.00	1588.00
μ(Mo Kα), cm^{-1}	12.57	13.32	26.69	7.54	7.88	7.08	8.67
diffractometer	CCD	RAXIS-CS	RAXIS-CS	CCD	CCD	RAXIS-RAPID	RAXIS-RAPID
radiation (λ, Å)	0.71069	0.71069	0.71069	0.71069	0.71069	0.71069	0.71069
temp, °C	25	−50	25	−50	−50	25	−50
GOF	1.831	1.683	1.210	2.694	2.756	1.610	1.849
no. of obsd data	877($I > 2.00\sigma(I)$)	579($I > 2.00\sigma(I)$)	537($I > 2.00\sigma(I)$)	3164($I > 2.00\sigma(I)$)	3347($I > 2.00\sigma(I)$)	3200($I > 2.00\sigma(I)$)	4871($I > 2.00\sigma(I)$)
no. of variables	81	48	81	461	470	197	433
R^a ($I > 2.00\sigma(I)$, all data)	0.0501, 0.0591	0.0548, 0.0648	0.0530, 0.1129	0.1009, 0.1143	0.0978, 0.1086	0.0615, 0.0767	0.0724, 0.0938
R_w^b ($I > 2.00\sigma(I)$, all data)	0.0751, 0.0786	0.0790, 0.0819	0.0550, 0.0640	0.1289, 0.1307	0.1272, 0.1288	0.0812, 0.0841	0.0914, 0.0963

[a] $R = \sum||F_o| - |F_c||/\sum|F_o|$. [b] $R_w = [(\sum w(|F_o| - |F_c|)^2/\sum wF_o^2)]^{1/2}$.

2.24 mmol). The obtained purple powder was filtered, washed with MeOH, and dried in air to give the microcrystals (yield; 579 mg, 88%). This compound easily released the guest H_2O molecules to form a partially dehydrated compound. The crystals suitable for the X-ray analysis were obtained as follows. An EtOH solution of 4,4′-bpy was diffused to an aqueous solution of $Cu(BF_4)_2\cdot xH_2O$ and $(NH_4)SiF_6$ in a straight glass tube. Purple crystals of **1a**·$8H_2O$ were obtained together with sky-blue crystals of **1b** after a few weeks. The homogeneity of the powder sample was confirmed by comparison of the observed and calculated XRPD patterns obtained from the single-crystal data. Anal. Calcd for $\{[Cu(SiF_6)(4,4'\text{-bpy})_2]\cdot 4H_2O\}_n$ (**1a**·$4H_2O$): C, 40.71; H, 4.10; N, 9.50. Found: C, 40.81; H, 3.50; N, 9.27. IR (KBr pellet): 3412 bm, 3098 w, 3045 w, 1610 m, 1535 w, 1493 w, 1412 w, 1221 w, 1078 w, 995 w, 812 s, 742 s, 644 m, 482 s (cm^{-1}).

The compound of **1b** was synthesized as follows. A hot aqueous solution (10 mL) of $Cu(BF_4)_2\cdot xH_2O$ (237 mg, 1.00 mmol) and $(NH_4)_2SiF_6$ (178 mg, 1.00 mmol) was added to a hot aqueous solution (10 mL) of 4,4′-bpy (312 mg, 2.00 mmol). The color of the resultant suspension was purple and gradually changed to sky-blue. The obtained sky-blue powder was filtered, washed with acetone, and dried in air to give the microcrystals (yield; 362 mg, 61%). The crystals suitable for the X-ray analysis were obtained by the same method as **1a**·$8H_2O$. The homogeneity of the powder sample was confirmed by comparison of the observed and calculated XRPD patterns obtained from the single-crystal data. This powder sample contains guest H_2O molecules, because of the presence of a vacant space generated by a slight defect of the overall structure. Anal. Calcd for $\{[Cu(4,4'\text{-bpy})_2(H_2O)_2]\cdot SiF_6\cdot 2.3H_2O\}_n$ (**1b**·$2.3H_2O$): C, 40.34; H, 4.16; N, 9.41. Found: C, 40.36; H, 3.78; N, 9.42. IR (KBr pellet): 3441 bm, 3109 w, 3088 w, 1635 w, 1612 s, 1537 w, 1493 w, 1415 m, 1223 m, 1068 m, 1014 w, 852 m, 812 m, 748 s, 690 s, 671 m, 642 m, 617 m, 480 m, 462 m (cm^{-1}).

Syntheses of $\{[Cu(GeF_6)(4,4'\text{-bpy})_2]\cdot 8H_2O\}_n$ (2a·$8H_2O$) and $\{[Cu(4,4'\text{-bpy})_2(H_2O)_2]\cdot GeF_6\}_n$ (2b). These compounds were prepared by a procedure similar to that of **1a**·$8H_2O$ and **1b** (yield; 65 and 62%, respectively). Anal. Calcd for $\{[Cu(GeF_6)(4,4'\text{-bpy})_2]\cdot 4H_2O\}_n$ (**2a**·$4H_2O$): C, 37.85; H, 3.81; N, 8.83. Found: C, 37.52; H, 3.48; N, 8.42. IR (KBr pellet): 3410 bm, 3098 m, 3045 m, 1610 s, 1535 w, 1493 w, 1412 m, 1332 w, 1221 m, 1111 m, 1076 m, 1045 w, 1012 w, 812 s, 723 w, 642 m, 607 s, 470 w (cm^{-1}). Anal. Calcd for $\{[Cu(4,4'\text{-bpy})_2(H_2O)_2]\cdot GeF_6\cdot 2.7H_2O\}_n$ (**2b**·$2.7H_2O$): C, 37.12; H, 3.96; N, 8.66. Found: C, 37.00; H, 3.58; N, 8.66. IR (KBr pellet): 3426 bm, 3111 w, 1637 w, 1610 s, 1537 w, 1493 w, 1415 m, 1323 w, 1223 w, 1068 m, 1014 w, 850 w, 812 m, 731 w, 679 w, 625 m, 603 s, 563 s, 470 w (cm^{-1}).

Synthesis of $\{[Cu_2(4,4'\text{-bpy})_5(H_2O)_4]\cdot 4PF_6\cdot 2H_2O\cdot 4EtOH\}_n$ (3·$2H_2O$·4EtOH). An EtOH solution (10 mL) of 4,4′-bpy (390 mg, 2.50 mmol) was diffused to an aqueous solution (10 mL) of $Cu(BF_4)_2\cdot xH_2O$ (237 mg, 1.00 mmol) and NH_4PF_6 (326 mg, 2.00 mmol) in a straight glass tube. Purple single crystals of **3**·$2H_2O$·4EtOH were obtained after a few days and collected. They were washed with EtOH and dried in air (yield; 85 mg, 10%). The crystals of **3**·$2H_2O$·4EtOH were also obtained together with sky-blue crystals of $\{[Cu(SO_4)(4,4'\text{-bpy})(H_2O)_3]\cdot 2H_2O\}_n$ (**8**·$2H_2O$) by using $CuSO_4\cdot 5H_2O$ as a starting material. This compound easily released guest H_2O and EtOH molecules to form a desolvated compound. Anal. Calcd for $\{[Cu_2(4,4'\text{-bpy})_5(H_2O)_4]\cdot 4PF_6\cdot 2EtOH\}_n$ (**3**·2EtOH): C, 39.26; H, 3.66; N, 8.48. Found: C, 38.72; H, 3.47; N, 8.47. IR (KBr pellet): 3395 w, 3117 w, 1684 w, 1616 m, 1539 w, 1493 w, 1425 m, 1226 w, 1076 m, 1022 w, 1001 w, 843 s, 814 s, 738 w, 669 w, 646 w, 639 w, 557 s (cm^{-1}).

Synthesis of $\{[Cu_2(4,4'\text{-bpy})_5(H_2O)_4]\cdot 2PF_6\cdot 2ClO_4\cdot 2H_2O\cdot 4EtOH\}_n$ (4·$2H_2O$·4EtOH). An EtOH solution (10 mL) of 4,4′-bpy (390 mg, 2.50 mmol) was diffused to an aqueous solution (10 mL) of $Cu(ClO_4)_2\cdot 6H_2O$ (370 mg, 1.00 mmol) and NH_4PF_6 (326 mg, 2.00 mmmol) in a straight glass tube. Purple single crystals of **4**·$2H_2O$·4EtOH were obtained after a few days and collected. They were washed with EtOH and dried in air (yield; 131 mg, 17%). This compound readily released the guest H_2O and EtOH molecules to form a desolvated compound. Anal. Calcd for $\{[Cu_2(4,4'\text{-bpy})_5(H_2O)_4]\cdot 2PF_6\cdot 2ClO_4\cdot 2EtOH\}_n$ (**4**·2EtOH): C, 41.55; H, 3.87; N, 8.97. Found: C, 41.02; H, 3.68; N, 9.09. IR (KBr pellet): 3422 w, 3113 w, 1616 m, 1558 w, 1539 w, 1491 w, 1423 w, 1224 w, 1115 m, 1076 m, 843 s, 814 s, 738 w, 669 m, 648 m, 625 m, 557 m (cm^{-1}).

Synthesis of $\{[Cu_2(PF_6)(NO_3)(4,4'\text{-bpy})_4]\cdot 2PF_6\cdot 2H_2O\}_n$ (5·$2PF_6$·$2H_2O$). An EtOH solution (20 mL) of 4,4′-bpy (312 mg, 2.00 mmol) was diffused to an aqueous solution (20 mL) of $Cu(NO_3)_2\cdot 3H_2O$ (242 mg, 1.00 mmol) and NH_4PF_6 (326 mg, 2 mmol) at the 1:2 ratio in a straight glass tube. Purple single crystals were obtained after a few days and collected. They were washed with EtOH and dried in air (yield; 150 mg, 23%). They are available for the single-crystal X-ray structure determination. According to the single-crystal structure, it contains only

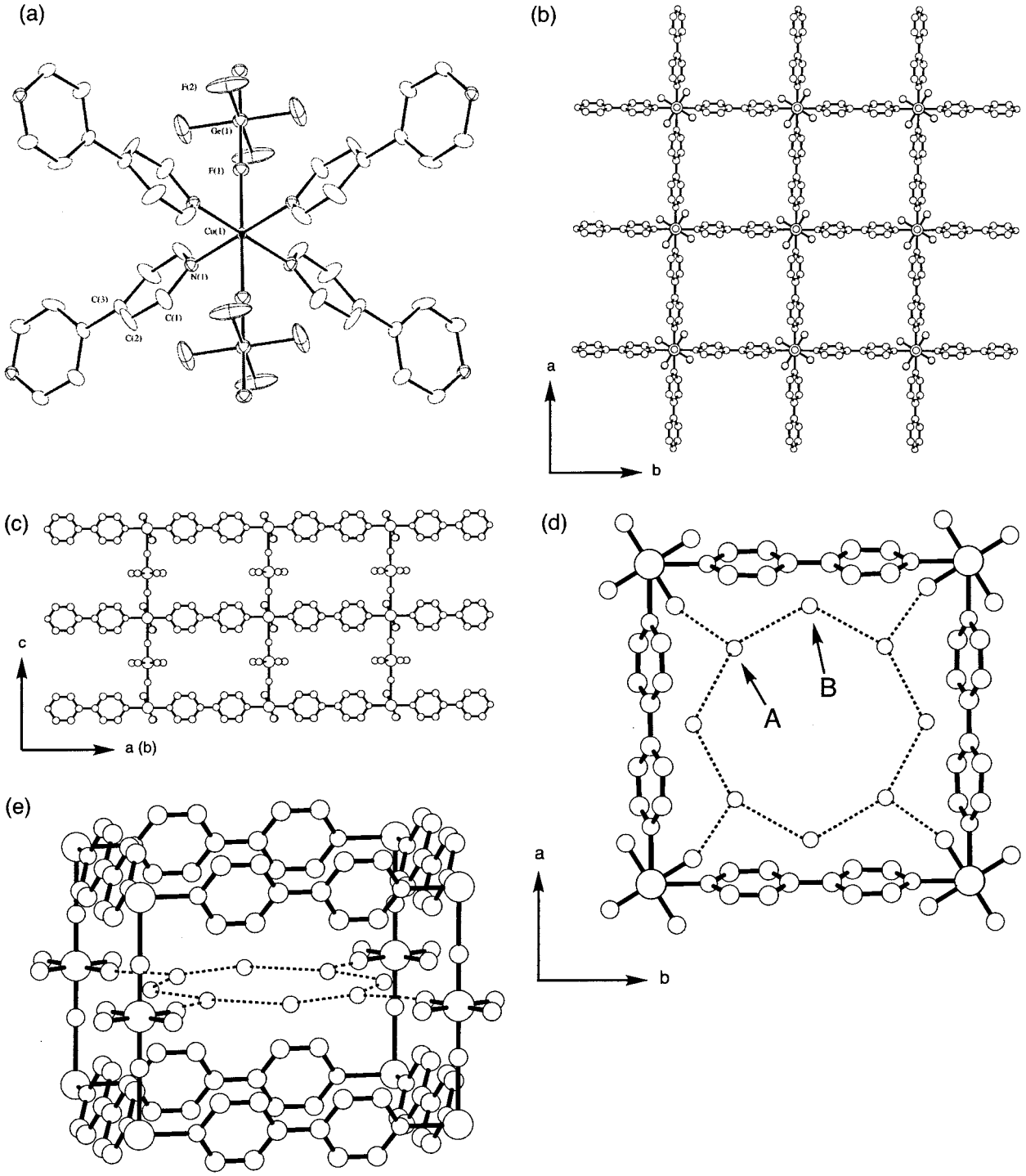

Figure 1. (a) ORTEP drawing around a Cu(II) center of **2a**·8H_2O at the 30% probability level. The hydrogen atoms, disordered pyridine carbon atoms, and disordered fluoro atoms are omitted for clarity. Selected bond distances (Å): Cu(1)−N(1) = 2.008(5), Cu(1)−F(1) = 2.320(5). (b and c) View of the microporous network of **2a**·8H_2O along the *c*-axis (b) and *a*- or *b*-axes (c). The guest H_2O molecules, the hydrogen atoms, disordered pyridine carbon atoms, and disordered fluoro atoms are omitted for clarity. (d and e) View of the eight-membered ring of guest H_2O molecules. The hydrogen atoms, disordered pyridine carbon atoms, and disordered fluoro atoms are omitted for clarity.

PF_6^- anions as metal-free counteranions in the channels. In the case of a large-scale preparation, partial replacement of the NO_3^- anions occurs for the free PF_6^- anions, and, therefore, the ratio of PF_6^- and NO_3^- anions in the elemental analysis is different from that of **5**·2PF_6·2H_2O. When a NO_3^- anion, with a smaller volume than that of PF_6^-, is included in the channel, an additional EtOH molecule is clathrated to occupy a vacant space of the channel. The XRPD pattern of the sample with mixed free counteranions is in agreement with the simulated pattern obtained from the X-ray crystal analysis of **5**·2PF_6·2H_2O, indicating the formation of the similar 3-D network. Anal. Calcd for {[$Cu_2(PF_6)$-$(NO_3)(4,4'\text{-bpy})_4$]·1.4$PF_6$·0.6$NO_3$·2$H_2O$·1.2EtOH}$_n$ (**5**·1.4PF_6·0.6NO_3·2H_2O·1.2EtOH): C, 39.47; H, 3.37; N, 10.42. Found: C, 39.55; H, 3.11; N, 10.44. IR (KBr pellet): 3421 bw, 3308 bw, 3113 w, 1705 w, 1645 w, 1616 m, 1537 w, 1495 w, 1421 m, 1385 m, 1348 m, 1321 m, 1228 w, 1107 w, 1070 w, 1020 w, 843 s, 738 w, 673 w, 646 m, 557 m (cm^{-1}).

Synthesis of {[Cu(PF_6)(4,4′-bpy)$_2$(MeCN)]·PF_6·2MeCN}$_n$ (6·2MeCN). A MeCN solution (10 mL) of 4,4′-bpy (312 mg, 2.00 mmol)

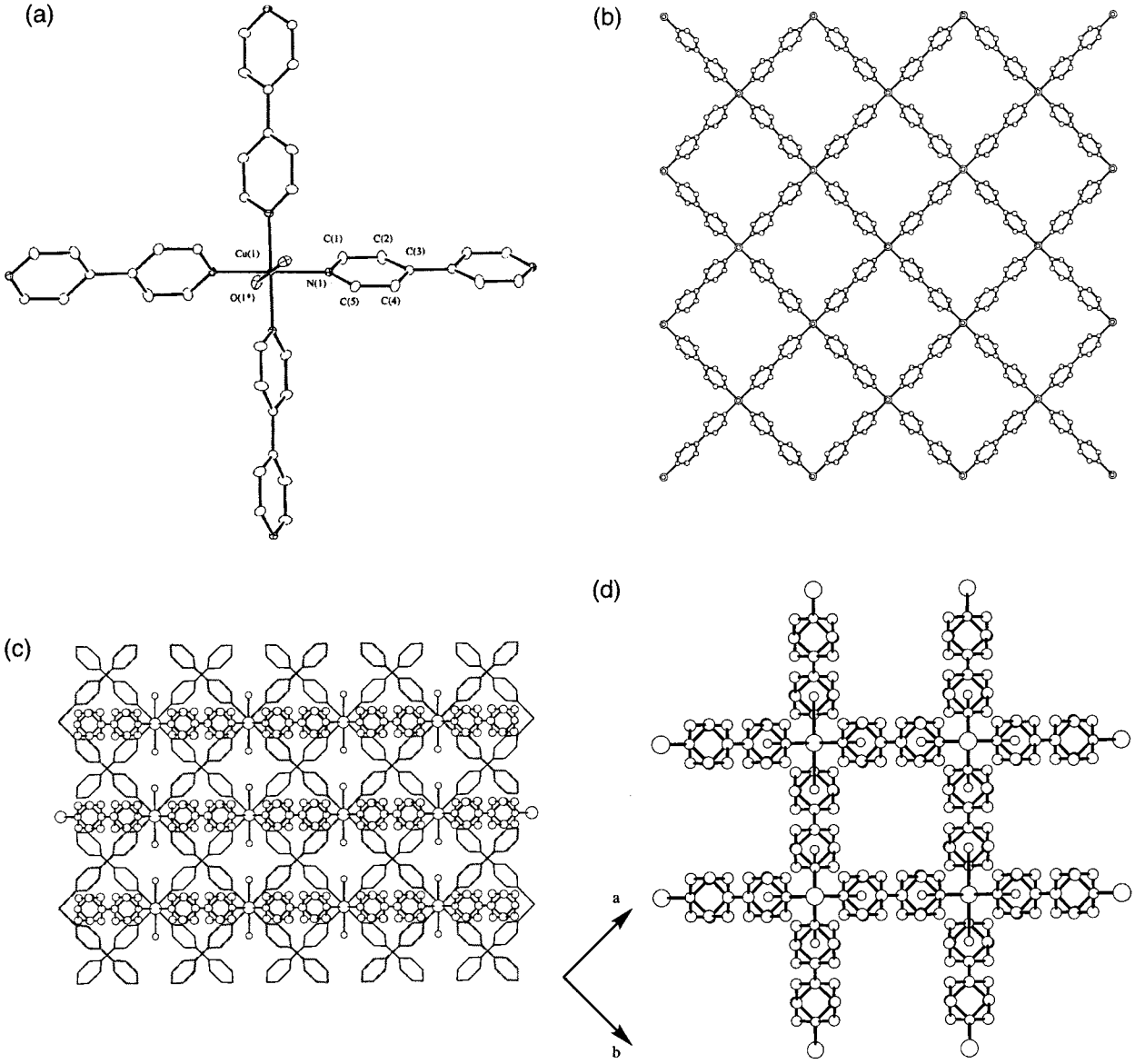

Figure 2. (a) ORTEP drawing around a Cu(II) center of **1b** at the 30% probability level. The hydrogen atoms are omitted for clarity. Selected bond distances (Å): Cu(1)−N(1) = 2.043(3), Cu(1)−O(1*) = 2.378(4) [Symmetry Code: (*) $x, y - 1, z$]. (b) View of a 2-D network of **1b** along the *ab* vector. The hydrogen atoms are omitted for clarity. (c) View of the interpenetration mode of **1b** along the *ab* vector. The two types of 2-D layers lying parallel and perpendicular to the paper plane are represented by the stick and cylindrical bond models, respectively. The counter SiF_6^{2-} anions and the hydrogen atoms are omitted for clarity. (d) View showing the micropore cross section of the network of **1b** along the *c*-axis. The counter SiF_6^{2-} anions and the hydrogen atoms are omitted for clarity.

was diffused to an aqueous solution (10 mL) of $Cu(BF_4)_2 \cdot xH_2O$ (237 mg, 1.00 mmol) and NH_4PF_6 (326 mg, 2.00 mmol) in a straight glass tube. Purple single crystals of **6**·2MeCN were obtained after a few days and collected. They were washed with MeCN and dried in air (yield; 132 mg, 17%). This compound readily released guest MeCN molecules and adsorbed ca. three molecules of H_2O in the atmosphere to form a hydrated compound $\{[Cu(PF_6)(4,4'\text{-bpy})_2(MeCN)] \cdot PF_6 \cdot 3H_2O\}_n$ (**6**·$3H_2O$). Anal. Calcd for $\{[Cu(PF_6)(4,4'\text{-bpy})_2(MeCN)] \cdot PF_6 \cdot 3H_2O\}_n$ (**6**·$3H_2O$): C, 34.73; H, 3.31; N, 9.20. Found: C, 34.37; H, 2.85; N, 9.21. IR (KBr pellet): 3431 bw, 1956 w, 1616 m, 1539 w, 1496 w, 1423 m, 1224 m, 1074 m, 1020 w, 839 s, 810 s, 738 w, 646 m, 557 m (cm^{-1}).

Synthesis of $\{[Cu(4,4'\text{-bpy})_2(H_2O)_2] \cdot PF_6 \cdot BF_4\}_n$ (7). A MeOH solution (10 mL) of 4,4′-bpy (312 mg, 2.00 mmol) was diffused to a MeOH solution (10 mL) of $Cu(BF_4)_2 \cdot xH_2O$ (237 mg, 1.00 mmol) and NH_4PF_6 (326 mg, 2.00 mmol) in a straight glass tube. Purple single crystals were obtained after a few days and collected. They were washed with MeOH and dried in air (yield; 144 mg, 22%). Anal. Calcd for $\{[Cu(4,4'\text{-bpy})_2(H_2O)_2] \cdot PF_6 \cdot BF_4\}_n$ (**7**): C, 37.32; H, 3.13; N, 8.70. Found: C, 37.37; H, 2.99; N, 8.88. IR (KBr pellet): 3437 bm, 3118 w, 1645 w, 1616 s, 1539 w, 1496 w, 1423 m, 1230 m, 1076 m, 1045 m, 976 w, 844 s, 819 s, 729 w, 648 w, 557 m, 482 w (cm^{-1}).

Synthesis of $\{[Cu(SO_4)(4,4'\text{-bpy})(H_2O)_3] \cdot 2H_2O\}_n$ (8·$2H_2O$). A MeOH solution (10 mL) of 4,4′-bpy (156 mg, 1.00 mmol) was added to an aqueous solution (10 mL) of $CuSO_4 \cdot 5H_2O$ (250 mg, 1.00 mmol). The obtained sky-blue powder was filtered, washed with H_2O and MeOH, and dried under vacuum for 2 h to give the microcrystals (yield; 363 mg, 89%). The homogeneity of the powder sample was confirmed by comparison of the observed XRPD pattern with a calculated pattern obtained from the single-crystal data reported previously.[62] Anal. Calcd for $\{[Cu(SO_4)(4,4'\text{-bpy})(H_2O)_3] \cdot 2H_2O\}_n$ (8·$2H_2O$): C, 29.59; H, 4.47; N, 6.90. Found: C, 29.77; H, 3.81; N, 6.82. IR (KBr pellet): 3422 bs, 1610 m, 1535 w, 1493 w, 1417 w, 1223 m, 1107 s, 1076 m, 1043 m, 968 w, 812 m, 723 w, 669 w, 646 m, 617 m, 472 w (cm^{-1}).

(62) Hagrman, D.; Hammond, R. P.; Haushalter, R.; Zubieta, J. *Chem. Mater.* **1998**, *10*, 2091−2100.

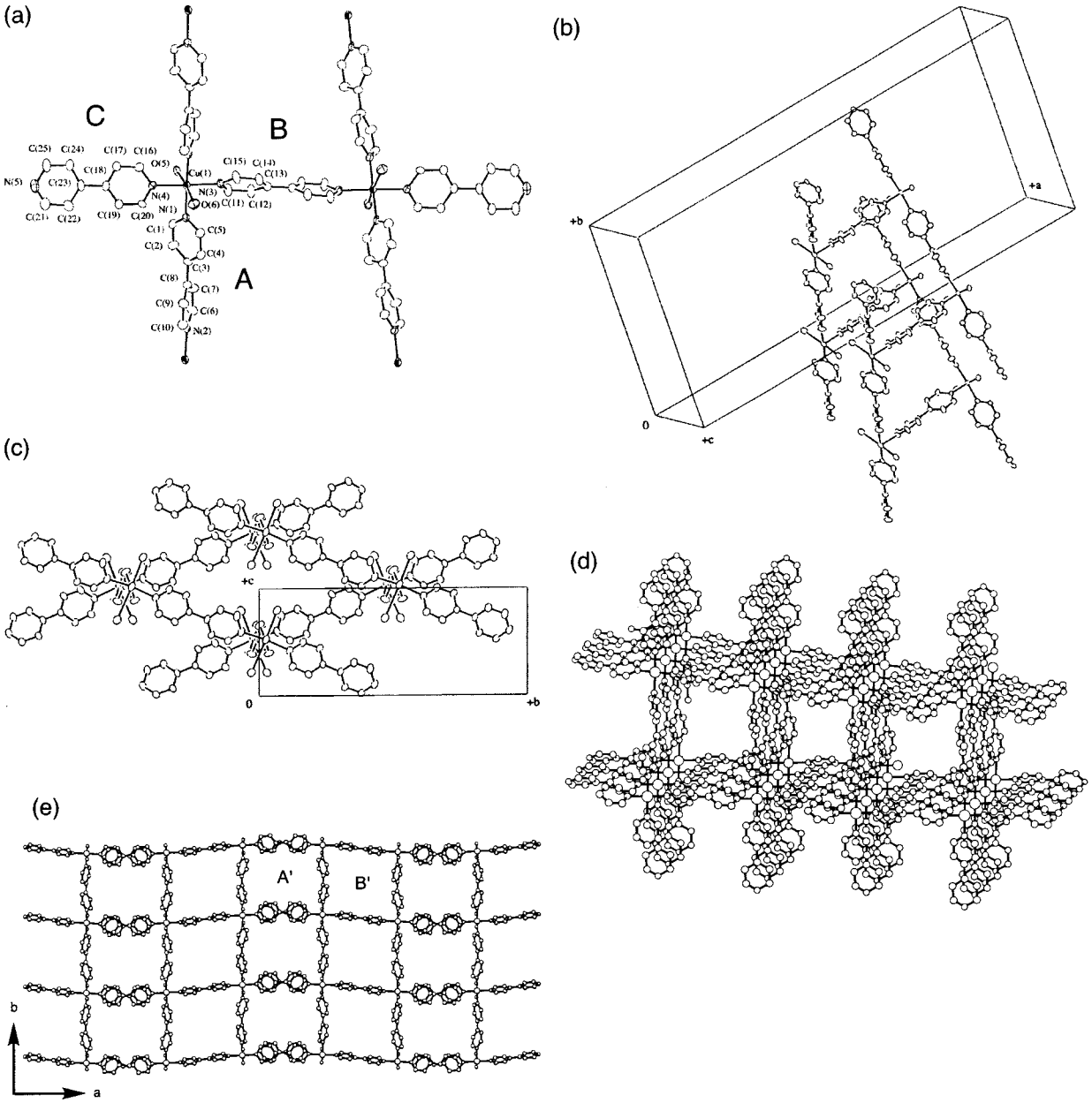

Figure 3. (a) ORTEP drawing around Cu(II) centers of **4**·2H_2O·4EtOH at the 30% probability level. The hydrogen atoms are omitted for clarity. Selected bond distances (Å): Cu(1)−N(1) = 1.985(8), Cu(1)−N(2*) = 1.986(8), Cu(1)−N(3) = 2.018(6), Cu(1)−N(4) = 1.994(6), Cu(1)−O(5) = 2.395(10), Cu(1)−O(6) = 2.73(1) [Symmetry Code: (*) x, $^1/_2 + y$, $-^1/_2 + z$]. (b and c) ORTEP view of the 4,4′-bpy ligands (mode B) bridging neighboring 1-D chains of **4**·2H_2O·4EtOH at the 30% probability level. The mode B of the 4,4′-bpy is directed to the *a*-axis. The hydrogen atoms (b and c) and the mode C of the 4,4′-bpy (only b) are omitted for clarity. (d) View of the 2-D thick network of **4**·2H_2O·4EtOH. The hydrogen atoms are omitted for clarity. (e) View showing the micropore cross section of the network of **4**·2H_2O·4EtOH along the *c*-axis. The counter PF_6^- and ClO_4^- anions, guest H_2O and EtOH molecules, and the hydrogen atoms are omitted for clarity.

Synthesis of {[Cu(4,4′-bpy)$_2$(H$_2$O)$_2$]·2PF$_6$}$_n$ (9). This compound was obtained by the anion-exchange reaction with **1b**. An excess amount of NH_4PF_6 was added to **1b** in an aqueous solution. After 3 days, a solution color changed from sky-blue to purple, and the resultant precipitate was filtered, washed with H_2O and acetone, and dried under vacuum for 2 h. Anal. Calcd for {[Cu(4,4′-bpy)$_2$(H$_2$O)$_2$]·2PF_6}$_n$ (**9**): C, 34.23; H, 2.87; N, 7.98. Found: C, 34.58; H, 2.54; N, 7.65. IR (KBr pellet): 3443 bw, 1616 m, 1539 w, 1496 w, 1423 w, 1327 w, 1226 w, 1074 w, 1020 w, 843 s, 814 m, 736 w, 648 w, 555 m, 505 w (cm^{-1}).

Results and Discussion

Crystal Structures of {[Cu(AF$_6$)(4,4′-bpy)$_2$]·8H$_2$O}$_n$ (A = Si (1a·8H$_2$O), Ge (2a·8H$_2$O)) and {[Cu(4,4′-bpy)$_2$(H$_2$O)$_2$]·AF$_6$}$_n$ (A = Si (1b), Ge (2b)). The crystallographic structure of **2a**·8H_2O clearly illustrates a 3-D network based on a square grid of [Cu(4,4′-bpy)$_2$]$_n$ and a pillar anion of GeF_6^{2-} and is similar to **1a**·8H_2O reported previously.[20] Figure 1a shows a coordination environment around a Cu(II) ion of **2a**·8H_2O. Four pyridyl nitrogen atoms of 4,4′-bpy ligands are coordinated to the Cu(II) ion. Association of two F atoms of the GeF_6^{2-} anions provides a (4 + 2) environment. The 4,4′-bpy ligands bridge Cu(II) ions to form a 2-D network of square grids. The layers are linked with GeF_6^{2-} anions by coordination bonds to give a 3-D structure without interpenetration (*3-D Regular Grid*). This network provides channels with dimensions of ca. 8 × 8 Å^2 along the *c*-axis and ca. 6 × 2 Å^2 along the *a*- and *b*-axes, as

shown in Figure 1b and c, respectively.[63] The channels are filled with eight crystallization H_2O molecules per one Cu(II) ion. In this crystal, there are two types of hydrogen bondings of the H_2O molecules. Four H_2O molecules (type A) are hydrogen-bonded to the F atoms of the GeF_6^{2-} ions and the nearest-neighbor H_2O molecules. The remaining four H_2O molecules (type B) link the type A of H_2O molecules to form an octangle ring (Figure 1d). These rings are located between Cu-4,4′-bpy layers as illustrated in Figure 1e.

An ORTEP view around a Cu(II) center of **1b** is shown in Figure 2a with a numbering scheme. The Cu(II) atom has an elongated octahedral environment with four nitrogen atoms of 4,4′-bpy ligands in the equatorial plane and two oxygen atoms of H_2O molecules in the axial sites. The Cu(II) centers are bridged by 4,4′-bpy ligands to form a 2-D sheet having square grids with corner angles of ca. 89 and 91° as shown in Figure 2b. Each 2-D sheet lying in the (a-b)c and (b-a)c planes affords a doubly interpenetration mode (*2-D Interpenetration*) to make microporous channels with dimensions of ca. 2×2 Å^2 along the *c*-axis (Figure 2c and d). These channels are filled by free SiF_6^{2-} dianions, which interact with the coordinated H_2O molecules by hydrogen bonds (2.702(3) Å). The complex **2b** also affords a similar network to **1b**, which is confirmed by the X-ray crystallographic determination. These compounds, **1a**·$8H_2O$ (**2a**·$8H_2O$) and **1b** (**2b**), are isostructural with the Zn(II) compounds reported previously.[64,65]

An interesting feature of these complexes is that the 3-D structures of **1a** and **2a** (*3-D Regular Grid*) are transformed into the 2-D interpenetrated structures of **1b** and **2b** (*2-D Interpenetration*), respectively, in the solid phase. When a solid sample of **1a** or **2a** was immersed in H_2O, the color changed from purple to sky-blue. The IR measurements show that A−F (A = Si and Ge) stretching bands of the sky-blue sample have a different frequency from those of the purple sample (from 742 to 748 cm^{-1} for Si, and from 607 to 563 cm^{-1} for Ge). Moreover, the XRPD patterns of the sky-blue powder are in good agreement with the simulated patterns calculated from the crystallographic data of **1b** and **2b**, clearly indicating that the 3-D porous coordination polymers, **1a** and **2a**, are transformed into the 2-D interpenetrated networks, **1b** and **2b**, respectively.

Crystal Structures of {[Cu_2(4,4′-bpy)$_5$(H_2O)$_4$]·anions·$2H_2O$·4EtOH}$_n$ (3·$2H_2O$·4EtOH (Anions = $4PF_6^-$); 4·$2H_2O$·4EtOH (Anions = $2PF_6^-$ and $2ClO_4^-$)). An ORTEP view around Cu(II) centers of **4**·$2H_2O$·4EtOH is illustrated in Figure 3a with the numbering scheme. The Cu(II) center has an elongated distorted octahedral environment with four 4,4′-bpy nitrogen atoms in the equatorial plane and two oxygen atoms of the H_2O molecules in the axial sites.

There are three modes of coordination for the 4,4′-bpy ligands as illustrated in Figure 3a. One is an infinite bridging mode (A), which links two Cu(II) atoms to form a linear chain. Another is a chain−chain bridging mode (B), which links the nearest-neighbor two chains. Interestingly, the 4,4′-bpy ligands (mode B) ligate these linear chains in a different direction (dihedral angle = ca. 44°) as shown in Figure 3b and c, resulting

Scheme 3

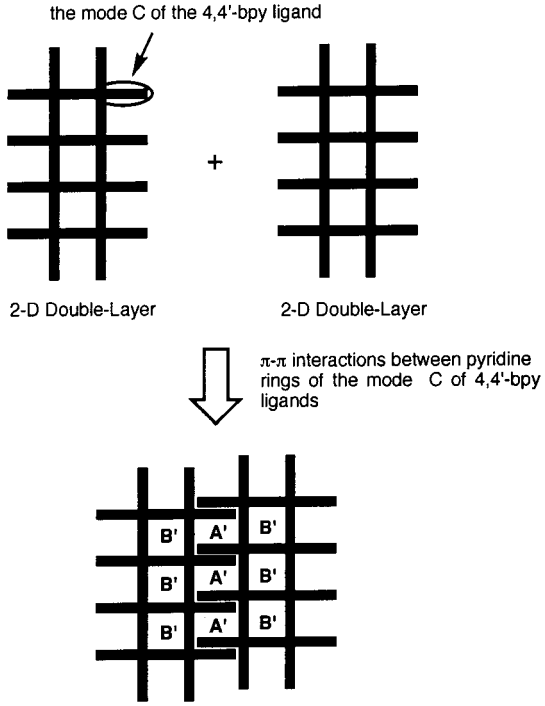

in a 2-D thick layer. The other is a terminal coordination mode (C), which is in a trans position to the mode B ligand. These three modes of the 4,4′-bpy afford an unprecedented 2-D structure (*2-D Double-Layer*) as illustrated in Figure 3d. This type of network is the first example in the 4,4′-bpy system,[5] although similar 2-D thick networks $[M_2(NO_3)_4(4,4'\text{-bpy})_3]_n$ (M = Co, Ni, Zn) have been found.[17,66,67] $[M_2(NO_3)_4(4,4'\text{-bpy})_3]_n$ networks afford a dihedral angle of ca. 60° between bridged 1-D chains, but an obvious difference is that the two NO_3^- anions ligate to the metal centers instead of to terminal 4,4′-bpy ligands in **4**·$2H_2O$·4EtOH. Therefore, stacking forms of these 2-D thick layers are apparently different from each other; the tongue-and-groove type stacking is seen for $[M_2(NO_3)_4(4,4'\text{-bpy})_3]_n$ while the $\pi-\pi$ stacking of terminal 4,4′-bpy ligands is seen for **4**·$2H_2O$·4EtOH.

Each 2-D thick layer assembles by $\pi-\pi$ stacking interactions between the mode C of the 4,4′-bpy to form a channeling network along the *c*-axis as shown in Figure 3e and Scheme 3. The shortest C···C separation, plane−plane angle, and angle between the ring normal of the pyridine plane and the ring−centroid vector are ca. 3.37 Å, 30°, and 11°, respectively.[68] Similar $\pi-\pi$ interaction has been reported in other 4,4′-bpy complexes.[69,70] In this crystal, there are two kinds of channels. One (A′) is defined by two 4,4′-bpy (mode C) ligands and two 2-D thick layers, and its channel size is ca. 7×3 Å^2. Another (B′) forms within the 2-D thick layer, and its size is ca. 6×6 Å^2. In the complex **4**·$2H_2O$·4EtOH, all PF_6^- anions are located in the channels A′, and all ClO_4^- anions are located in the channels B′. The guest H_2O and EtOH molecules are also included in the channels, and no bonding interactions with the

(63) Hereafter the channel dimensions are calculated by considering overlapping spheres with van der Waals radii.
(64) Subramanian, S.; Zaworotko, M. J. *Angew. Chem., Int. Ed. Engl.* **1995**, *34*, 2127−2129.
(65) Gable, R. W.; Hoskins, B. F.; Robson, R. *Chem. Commun.* **1990**, 1667−1668.
(66) Power, K. N.; Hennigar, T. L.; Zaworotko, M. J. *New J. Chem.* **1998**, 177−181.
(67) Kepert, C. J.; Rosseinsky, M. J. *Chem. Commun.* **1999**, 375−376.
(68) Janiak, C. *J. Chem. Soc., Dalton Trans.* **2000**, 3885−3896.
(69) Noro, S.; Kondo, M.; Ishii, T.; Kitagawa, S.; Matsuzaka, H. *J. Chem. Soc., Dalton Trans.* **1999**, 1569−1574.
(70) Tong, M.-L.; Lee, H.-K.; Chen, X.-M.; Huang, R.-B.; Mak, T. C. W. *J. Chem. Soc., Dalton Trans.* **1999**, 3657−3659.

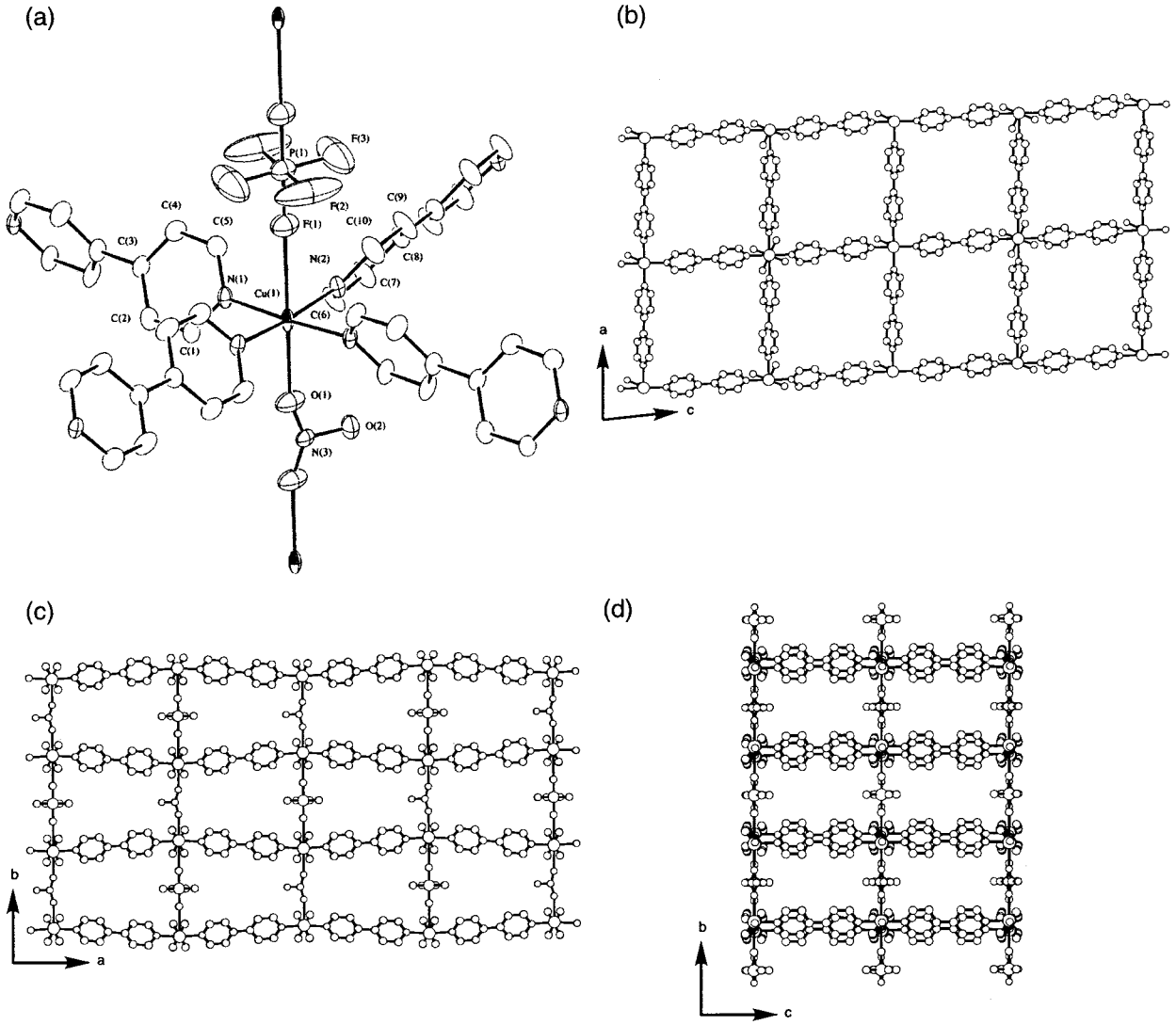

Figure 4. (a) ORTEP drawing around a Cu(II) center of **5**·2PF_6·2H_2O at the 30% probability level. The hydrogen atoms are omitted for clarity. Selected bond distances (Å): Cu(1)−N(1) = 2.028(2), Cu(1)−N(2) = 2.023(2), Cu(1)−O(1) = 2.320(5), Cu(1)−F(1) = 2.676(4). (b−d) View of the microporous network of **5**·2PF_6·2H_2O along the *b*- (b), *c*- (c), and *a*-axes. The free PF_6^- anions, guest H_2O molecules, and the hydrogen atoms are omitted for clarity.

host network are observed. The crystal structure of **3**·2H_2O·4EtOH is similar to that of **4**·2H_2O·4EtOH.

Crystal Structure of {[$Cu_2(PF_6)(NO_3)$(4,4′-bpy)$_4$]·2PF_6·2H_2O}$_n$ (5·2PF_6·2H_2O). An ORTEP view around a Cu(II) center of **5**·2PF_6·2H_2O is shown in Figure 4a with the numbering scheme. The Cu(II) atom has an elongated distorted octahedral environment with four 4,4′-bpy nitrogen atoms in the equatorial plane and one oxygen atom of the NO_3^- anion and one fluoro atom of the PF_6^- anion in the axial sites. The Cu−F distance (2.676(4) Å) is far longer than the Cu−O distance (2.320(5) Å), indicative of a weak coordination ability of the PF_6^- anion. Interestingly, the Cu−F distance of **5**·2PF_6·2H_2O is longer than those of **1a**·8H_2O (2.357(3) Å) and **2a**·8H_2O (2.320(5) Å), exhibiting that the interaction of Cu^{2+}···F could be modulated for infinite networks even though the principal origin is electrostatic.

The 4,4′-bpy ligands bridge Cu(II) ions to form a 2-D network of rhombus grids with the corner angles of ca. 86° and 94° as shown in Figure 4b. The layers are linked alternately with NO_3^- and PF_6^- anions by coordination bonds to give a 3-D structure without interpenetration (*3-D Undulated Grid*). Since the Cu···Cu bridging distances of NO_3^- and PF_6^- anions are different from each other (Cu···NO_3···Cu distance = 6.807 Å; Cu···PF_6···Cu distance = 8.506 Å), the 2-D sheets of [Cu(4,4′-bpy)$_2$]$_n$ undulate as shown in Figure 4c. This network provides channels with dimensions of ca. 7 × 7 Å^2 along the *b*-axis, ca. 6 × 3 Å^2 along the *c*-axis, and ca. 6 × 2 Å^2 along the *a*-axis as shown in Figure 4b−d. The 3-D network of **5**·2PF_6·2H_2O is very similar to those of **1a**·8H_2O and **2a**·8H_2O, but the remarkable difference is the valence of the counteranions. In **1a**·8H_2O and **2a**·8H_2O, the 2-D sheets are bridged by the dianions (SiF_6^{2-} or GeF_6^{2-}) to form a neutral 3-D network. On the other hand, the 2-D sheets of **5**·2PF_6·2H_2O are linked by the monoanions (NO_3^- and PF_6^-) to afford a cationic 3-D network of [$Cu_2(PF_6)(NO_3)$(4,4′-bpy)$_4$]$_n^{2+}$. Thus, the additional metal-free anions PF_6^- are contained in the channels, which are located near the bridging NO_3^- anions, and the effective channel sizes are ca. 4 × 3 Å^2 along the *b*-axis and ca. 3 × 3 Å^2 along the *c*-axis. As a result, 3 mol of PF_6^- and 1 mol of NO_3^- per 1 mol of **5**·2PF_6·2H_2O exist in the crystal. The IR stretching bands of both PF_6^- and NO_3^- anions are observed, consistent with the structure. The guest H_2O molecules sit in

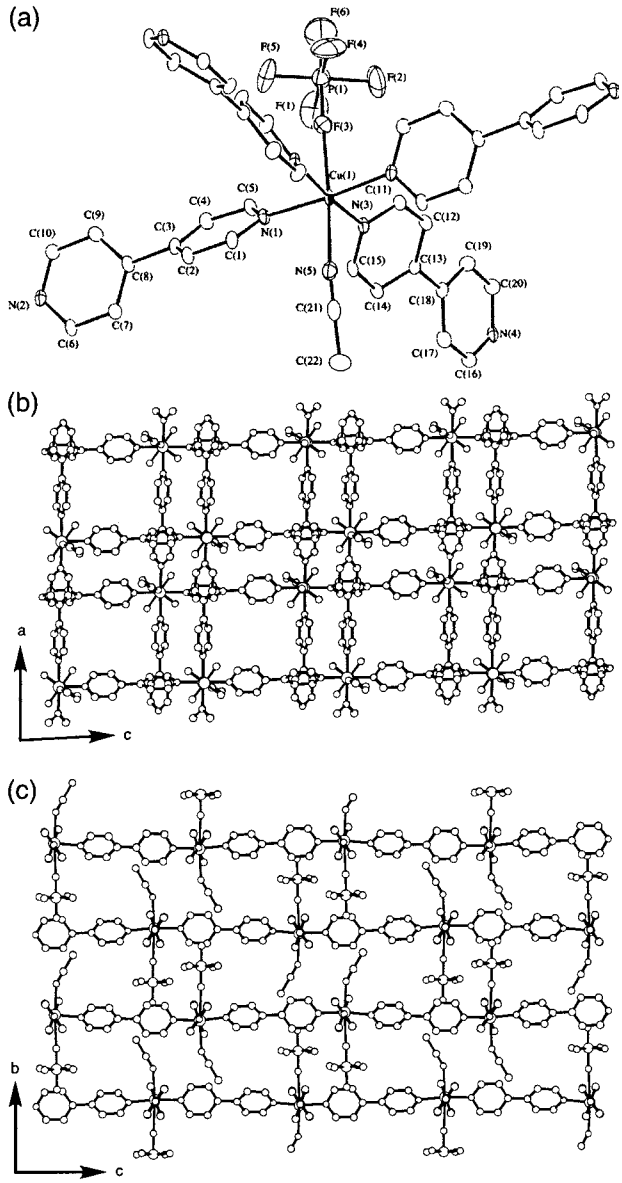

Figure 5. (a) ORTEP drawing around a Cu(II) center of **6**·2MeCN at the 30% probability level. The hydrogen atoms are omitted for clarity. Selected bond distances (Å): Cu(1)−N(1) = 2.055(3), Cu(1)−N(2*) = 2.044(3), Cu(1)−N(3) = 2.028(3), Cu(1)−N(4**) = 2.021(3), Cu(1)−N(5) = 2.399(5), Cu(1)−F(3) = 2.583(3) [Symmetry Code: (*) $x - 1, y, z$; (**) $x, {}^1/_2 - y, -{}^1/_2 + z$]. (b and c) View of the microporous network of **6**·2MeCN along the *b*- (b) and *a*- (c) axes. The free PF_6^- anions, guest MeCN molecules, and the hydrogen atoms are omitted for clarity.

the channels with a distance of on average 4.00 Å for the bridging PF_6^- anions. No bonding interaction is observed between the 3-D network and H_2O molecules. It is worth noting that **5**·2PF_6·2H_2O is the first example which has a mixed-pillar structure.

Crystal Structure of {[Cu(PF_6)(4,4′-bpy)$_2$(MeCN)]·PF_6·2MeCN}$_n$ (6·2MeCN). An ORTEP view around a Cu(II) center of **6**·2MeCN is shown in Figure 5a with the numbering scheme. The Cu(II) atom has an elongated distorted octahedral environment with four 4,4′-bpy nitrogen atoms in the equatorial plane and one nitrogen atom of the MeCN and one fluoro atom of the PF_6^- in the axial sites. The Cu−F distance (2.583(3) Å) of **6**·2MeCN is apparently shorter than that of **5**·2PF_6·2H_2O (2.676(4) Å), associated with the terminal coordination mode of the PF_6^- anion.

The 4,4′-bpy ligands bridge Cu(II) ions to form a 2-D network of rhombus grids with corner angles of ca. 87° and 93°. No significant bonding interactions are observed between the 2-D sheets except for a short F···F contact with the distance (2.879(8) Å) of coordinated PF_6^- anions in the neighboring sheets. The F···F contact is comparable to that of a F_2 solid,[71] implying the presence of a weak interaction between the 2-D sheets. These layers mutually slide to form small channels with dimensions of ca. 3 × 4 Å^2 along the *b*-axis and ca. 3 × 2 Å^2 along the *a*-axis as shown in Figure 5b and c. These channels are filled with free PF_6^- anions, which show no interactions with the host network. Two free guest MeCN molecules are located between the 2-D layers and in the channels, respectively.

Participation of PF_6^- Anion in Frameworks. Three types of participation of PF_6^- anion are observed in the frameworks. The first is coordination-free type, which is usual phenomena for coordination polymers containing PF_6^- anions reported so far. The second is bridging type, which is first observed in complex **5**·2PF_6·2H_2O. The third is terminal coordination type (**6**·2MeCN), whose examples are still sparse to date.[72−74] The PF_6^- anion has poor coordination ability for usual transition metal ions, hardly providing complexes with a direct bond between a metal atom and a fluorine atom. In the case of Cu(II) complexes, which undergo Jahn−Teller distortion and give a (4 + 2) coordination environment, PF_6^- anions could occupy the axial sites of the Cu(II) ion. This finding in **5**·2PF_6·2H_2O indicates that the PF_6^- anion is also effective for the construction of the 3-D porous network as well as AF_6^{2-} (A = Si, Ge) anions in the Cu(II)/4,4′-bpy system.[20] The evaluation of the porous properties is mentioned below.

Coexistent Effect of Counteranions in Porous Coordination Polymers Containing PF_6^- Anions. For the synthesis, Cu(PF_6)$_2$ could not be utilized because it was not commercially available. Therefore, the mixture of NH_4PF_6 with appropriate Cu salt such as Cu(ClO_4)$_2$·6H_2O, $CuSO_4$·5H_2O, Cu(BF_4)$_2$·*x*H_2O, and Cu(NO_3)$_2$·3H_2O was used as a starting salt. The frameworks of obtained complexes are considerably dependent on the combination of anions. A summary is shown in Scheme 2. When Cu(ClO_4)$_2$·6H_2O and NH_4PF_6 were employed in the reaction with 4,4′-bpy ligand in a H_2O/EtOH solution, the cationic coordination polymer, **4**·2H_2O·4EtOH, containing both ClO_4^- and PF_6^- anions at the 1:1 ratio was selectively obtained. The coexistence of counteranions is checked by the IR measurement, which shows the peaks of both 1115 and 843 cm^{-1} assigned to stretching bonds of ClO_4^- and PF_6^-, respectively. However, a combination of Cu(BF_4)$_2$·*x*H_2O or $CuSO_4$·5H_2O with NH_4PF_6 in a H_2O/EtOH solution afforded isostructural cationic coordination polymers **3**·2H_2O·4EtOH. In this compound, only PF_6^- anions are clathrated in the channels, in contrast to the case of Cu(ClO_4)$_2$·6H_2O. When the Cu(NO_3)$_2$·3H_2O and NH_4PF_6 were used in a H_2O/EtOH solution, the cationic 3-D coordination polymer **5**·2PF_6·2H_2O containing both NO_3^- and PF_6^- anions at the 1:3 ratio was formed. Interestingly, both bridged and free PF_6^- anions occur at the 1:2 ratio. A combined action of solvent molecules and anions was observed in the PF_6^-/BF_4^- system.

(71) Greenwood, N. N.; Earnshaw, A. *Chemistry of the Elements*, 2nd ed.; Butterworth-Heinemann: Oxford, 2001; p 803.
(72) Yamamoto, Y.; Aoki, K.; Yamazaki, H. *Inorg. Chim. Acta* **1983**, *68*, 75−78.
(73) Dartiguenave, M.; Dartiguenave, Y.; Mari, A.; Guitard, A.; Olivier, M. J.; Beauchamp, A. L. *Can. J. Chem.* **1988**, *66*, 2386−2394.
(74) Honeychuck, R. V.; Hersh, W. H. *Inorg. Chem.* **1989**, *28*, 2869−2886.

Both MeCN and PF_6^- anions are coordinated to Cu(II) atoms to give a 2-D coordination polymer **6**·2MeCN with both terminal-coordinated and free PF_6^- anions. However, in the absence of MeCN, **7** forms preferentially. On the basis of this, the combination of anions in a certain solvent provides a variety of infinite frameworks even for the simple Cu(II) ion and 4,4′-bpy system, indicating that the framework is designable and controllable. Crystalline frameworks depending on a single anion have so far been reported,[75−81] and, in addition, the finding on framework transformation by the combination of anions makes crystal engineering by anions promising.

Framework Stability. The stability of porous networks was studied by XRPD measurements and thermal gravimetric analyses (TGA). The XRPD pattern of dehydrated sample can be reproduced by simulation based on the single-crystal data with no crystallized water molecules. The TGA data of **1a**·$x$$H_2O$ reveal that the guest H_2O molecules are removed until ca. 100 °C and the decomposition of the porous framework is observed up to ca. 150 °C. The XRPD pattern was measured at 100 °C under vacuum. The good agreement of the peaks in both the simulation and the observed pattern demonstrates that the porous network is retained in the absence of any guest molecules in the channels. Similar results were observed in **2a**·$x$$H_2O$. Further evidence for the stability of the framework was obtained by heating the solvated crystals **1a**·8H_2O at 80 °C for 1 h, which had no effect on either their morphology or their crystallinity. The cell parameters obtained are unaltered relative to those found for the unheated solvated crystals, illustrating the robustness of the framework in the absence of guest molecules.[82] This heated sample $\{[Cu(SiF_6)(4,4'\text{-bpy})_2]\cdot 5H_2O\}_n$ (**10**·5H_2O) includes 5 mol of H_2O molecules per 1 mol of the Cu(II) atom. This is because moisture in the atmosphere promotes readsorption of H_2O in the vacant channels. The readsorbed H_2O molecules are also located in SiF_6^{2-} layers and incorporated in a linear fashion along the *a*- and *b*-axes.

In other porous compounds, only **6**·2MeCN showed the replacement of three H_2O from two MeCN, resulting in **6**·3H_2O. Therefore, we examined the framework stability of this replaced compoundin detail. For **6**·3H_2O, the TGA data show three steps of weight loss. First, at the region from room temperature to 70 °C, **6**·3H_2O loses three H_2O molecules. Immediately, the coordinated MeCN molecule is released from the host network between 70 and 127 °C, and the decomposition of the host network is observed up to 200 °C. The elemental analysis, IR, and TGA measurements reveal that guest MeCN molecules of the complex **6**·2MeCN are easily replaced by H_2O molecules in the atmosphere. The XRPD pattern of this replaced complex **6**·3H_2O was measured, and the good agreement of peaks in both simulation and observed patterns at room temperature demonstrates that the porous network is retained after the replacement by H_2O molecules in the atmosphere.

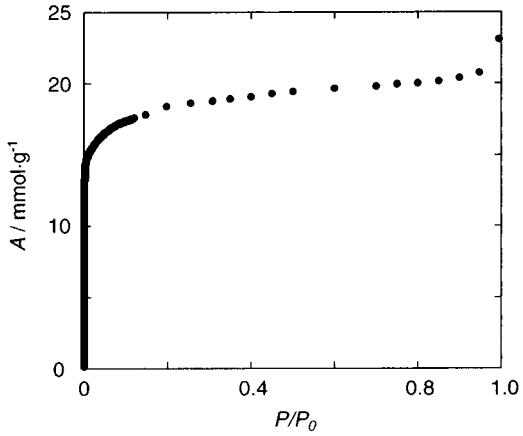

Figure 6. Adsorption isotherm of **1a** obtained with an argon gas in the relative pressure range from 10^{-6} to 1 at −185.7 °C (A = absolute adsorption (mmol g^{-1})).

Gas Adsorption Properties of 3-D Porous Coordination Polymers (1a, 2a, and 5·1.4PF_6·0.6NO_3). The 3-D porous coordination polymers **1a** and **2a** are useful for the adsorbtion of several gases. For **1a**, the argon adsorption experiment was carried out in the relative pressure range from 10^{-6} to 1 at −185.7 °C (Figure 6). This compound shows an isotherm of type I, indicative of a typical microporous compound. The isotherm displays a rapid rise at low relative pressure followed by a monotonically increasing curve. This is attributed to the uniform micropore, characteristic of metal−organic frameworks. The micropore filling of vapors is well described by the following Dubinin−Radushkevich (DR) equation:

$$[\ln(W_0/W)]^{1/2} = (RT/\beta E_0)(\ln(P_0) - \ln(P)) \qquad (1)$$

Here the parameters W and W_0 are the amount of adsorption at P/P_0 and the pore volume, respectively. βE_0 is the adsorption potential, in which β and E_0 are the affinity coefficient and characteristic adsorption energy, respectively. The DR plot is almost linear in the higher P/P_0 region, giving the micropore volume W_0 = 16.9 mmol g^{-1} and βE_0 = 10.3 kJ mol^{-1}. Furthermore, the βE_0 leads to the isosteric heat of adsorption $q_{st,\phi=1/e}$ at the fractional filling of 1/e by the following equation:

$$q_{st,\phi=1/e} = \Delta H_v + \beta E_0 \qquad (2)$$

where ΔH_v is the heat of vaporization of bulk liquid. The $q_{st,\phi=1/e}$ value is 16.8 kJ mol^{-1}, whose value is comparable with those of porous coordination polymers $[Cu(dicarboxylate)]_n$ (dicarboxylate = fumarate, terephthalate, and *trans*-1,4-cyclohexanedicarboxylate).[24]

The surface area and pore size distribution of **1a** were calculated from argon gas adsorption at −185.7 °C according to the BET equation and Horvath−Kawazoe (HK) method,[83] respectively. The differential pore volume plot, represented by the HK method, shows a single sharp peak around 8 Å. This compound possesses quite a uniform square pore (8 × 8 $Å^2$),

(75) Withersby, M. A.; Blake, A. J.; Champness, N. R.; Hubberstey, P.; Li, W. S.; Schröder, M. *Angew. Chem., Int. Ed. Engl.* **1997**, *36*, 2327−2329.
(76) Hirsch, K. A.; Wilson, S. R.; Moore, J. S. *Inorg. Chem.* **1997**, *36*, 6, 2960−2968.
(77) Carlucci, L.; Ciani, G.; Macchi, P.; Proserpio, D. M.; Rizzato, S. *Chem.-Eur. J.* **1999**, *5*, 237−243.
(78) Wu, H.-P.; Janiak, C.; Rheinwald, G.; Hang, H. *J. Chem. Soc., Dalton Trans.* **1999**, 183−190.
(79) Janiak, C.; Uehlin, L.; Wu, H.-P.; Klüfers, P.; Piotrowski, H.; Scharmann, T. G. *J. Chem. Soc., Dalton Trans.* **1999**, 3121−3131.
(80) Blake, A. J.; Champness, N. R.; Cooke, P. A.; Nicolson, J. E. B.; Wilson, C. *J. Chem. Soc., Dalton Trans.* **2000**, 3811−3819.
(81) Brooks, N. R.; Blake, A. J.; Champness, N. R.; Cunningham, J. W.; Hubberstey, P.; Teat, S. J.; Wilson, C.; Schröder, M. *J. Chem. Soc., Dalton Trans.* **2001**, 2530−2538.
(82) The heated single-crystal **10**·5H_2O was analyzed at −100 °C: Tetragonal, space group *P*4/*mmm* with a = 11.0449(6) Å, c = 8.055(1) Å, V = 982.6(1) $Å^3$, Z = 1, ρ(calcd) = 1.027 g cm^{-3}, F(000) = 311.00, μ(Mo Kα) = 6.40 cm^{-1}, no. of obsd data = 447, no. of variables = 44, R(I > 2.00σ(I), all data) = 0.1231, 0.1529, R_w (I > 2.00σ(I), all data) = 0.1557, 0.1609, GOF = 2.250.
(83) Horvath, G.; Kawazoe, K. *J. Chem. Eng. Jpn.* **1983**, *16*, 470−475.

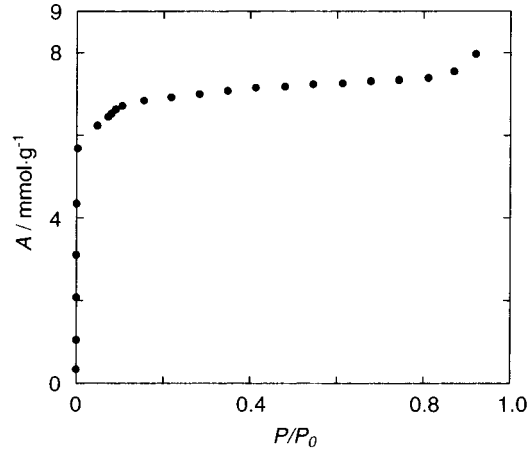

Figure 7. Adsorption isotherm of **5**·1.4PF_6·0.6NO_3 obtained with nitrogen gas in the relative pressure range from 10^{-6} to 0.9 at −196 °C (A = absolute adsorption (mmol g^{-1})).

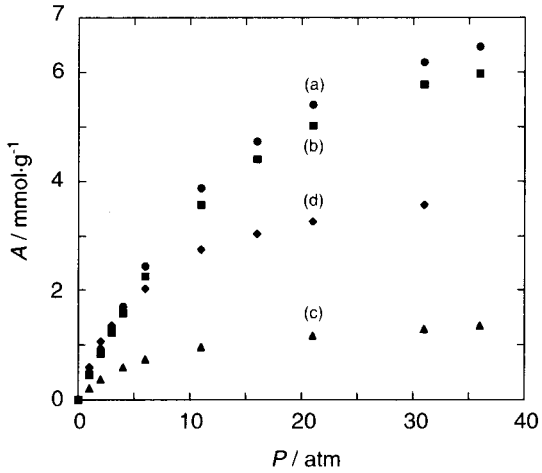

Figure 8. Adsorption isotherms of (a) **1a**, (b) **2a**, (c) **5**·1.4PF_6·0.6NO_3, and (d) zeolite 5A, obtained with a methane gas between 1 and 36 atm at 25 °C (A = absolute adsorption (mmol g^{-1})).

which is in fairly good agreement with the crystallographic structure. This plot also shows that argon molecules cannot pass through the rectangular pore (6 × 2 Å^2) at −185.7 °C because of the larger diameter of argon. The specific surface area from argon adsorption is calculated to be 1337 m^2 g^{-1}.

The nitrogen adsorption measurement of **5**·1.4PF_6·0.6NO_3 was carried out in the relative pressure range from 10^{-6} to 0.9 at −196 °C (Figure 7). This also shows a typical isotherm of type I for microporous compounds. The rapid rise at low relative pressure followed by a monotonically increasing curve indicates a uniform micropore. From eqs 1 and 2, the values of W_0 = 6.5 mmol g^{-1}, βE_0 = 10.1 kJ mol^{-1}, and $q_{st,\phi=1/e}$ = 15.7 kJ mol^{-1} are estimated. The value of the specific surface area of **5**·1.4PF_6·0.6NO_3, which is calculated from the BET equation, is 559 m^2 g^{-1}.

The methane adsorption experiments of **1a** and **2a** were also carried out in comparison with zeolite 5A, which has the highest methane adsorption capacity in zeolites.[56,84,85] Figure 8 shows the isotherms for the methane adsorption in the pressure range between 1 and 36 atm at 25 °C. The methane adsorption quantity at high pressure in **1a** (ca. 6.5 mmol g^{-1} at 36 atm) is much larger than that of zeolite 5A (ca. 3.7 mmol g^{-1} at 36 atm). At 36 atm, the density of methane adsorbed in **1a** for micropore volume is 0.21 g mL^{-1}. The density of the compressed methane gas at 27 °C and 280 atm (0.16 g mL^{-1}) is almost the same as that of **1a** at 25 °C and 36 atm, indicative of a concentration effect by strong micropore filling in the cavities. The high-pressure adsorption of supercritical methane in the micropore field has been studied with the following extended DR equation:[86,87]

$$[\ln(W_L/W)]^{1/2} = (RT/\beta E_0)(\ln(P_{0q}) - \ln(P)) \qquad (3)$$

Here the parameters W_L and P_{0q} are the inherent micropore volume and the saturated vapor pressure of the quasi-vaporized supercritical methane, respectively. The large inherent micropore volume W_L of 10.0 mmol g^{-1} is obtained from the Langmuir plot. This isotherm is well explained by this extended DR equation. The obtained parameters βE_0 and P_{0q} are 8.0 kJ mol^{-1} and 284 atm, respectively. The porous compound **2a** similar to **1a** also adsorbs a large amount of the methane gas (ca. 6.0 mmol g^{-1} at 36 atm). The obtained parameters W_L, βE_0, and P_{0q} are 9.47 mmol g^{-1}, 8.0 kJ mol^{-1}, and 290 atm, respectively, comparable to those of **1a**. The $q_{st,\phi=1/e}$ value of 16.2 kJ mol^{-1}, calculated from eq 2, is similar to those of activated carbon (17.6 kJ mol^{-1}),[88] activated carbon fibers (17−18 kJ mol^{-1}),[86] and the porous coordination polymer $[Cd_2(NO_3)_4(azpy)_3]_n$ (16.3 kJ mol^{-1}) (azpy = 4,4′-azopyridine).[19] However, the $q_{st,\phi=1/e}$ values of **1a** and **2a** are apparently smaller than that of $[Co(NCS)_2(azpy)_2]_n$ (20.2 kJ mol^{-1}),[19] because the interpenetrated coordination polymer $[Co(NCS)_2(azpy)_2]_n$ affords very small channels (ca. 3 × 3 Å^2) and has a deeper potential well than those of **1a** and **2a**. The 3-D cationic porous coordination polymer **5**·1.4PF_6·0.6NO_3 also contains small channels (4 × 3 Å^2 and ca. 3 × 3 Å^2). This dried sample adsorbs a small amount of the methane gas (ca. 1.4 mmol g^{-1} at 36 atm). The parameters obtained from the Langmuir plot and the extended DR equation W_L, βE_0, and P_{0q} are 1.58 mmol g^{-1}, 8.8 kJ mol^{-1}, and 146 atm, respectively. The $q_{st,\phi=1/e}$ value of 17.0 kJ mol^{-1} is comparable with those of **1a** and **2a**.

Micropore filling of argon, nitrogen, and supercritical methane is physical adsorption enhanced by the micropore field and has a greater heat of adsorption than typical physical adsorption on the flat surface by several kJ mol^{-1}. Therefore, the enhancement of the micropore filling strongly depends on the micropore width and shape. For instance, the cross section of a channel illustrates the adsorption capacity for which the size 4 × 4 Å^2 is well-suited and thus has a larger affinity for a methane molecule than that of 12 × 12 Å^2. However, the size of 12 × 12 Å^2 is relevant for the adsorption capacity because of the large porosity. As mentioned above, coordination polymers can easily afford channels of nanometric size by crystal engineering, potentially being a good candidate for a new adsorbent.

Crystal Engineering by Anions for Cu(II)/4,4′-bpy Frameworks. The framework construction and conversion accompanied by anion-exchange are listed in Scheme 4.

(84) Zhang, S.-Y.; Talu, O.; Hayhurst, D. T. *J. Phys. Chem.* **1991**, *95*, 1722−1726.
(85) Zuech, J. L.; Hines, A. L.; Sloan, E. D. *Ind. Eng. Chem. Process Des. Dev.* **1983**, *22*, 172−174.
(86) Kaneko, K.; Murata, K.; Shimizu, K.; Camara, S.; Suzuki, T. *Langmuir* **1993**, *9*, 1165−1167.
(87) Kaneko, K.; Murata, K. *Adsorption* **1997**, *3*, 197−208.
(88) Agarwal, R. K.; Schwarz, J. A. *J. Colloid Interface Sci.* **1989**, *130*, 137−145.

Scheme 4

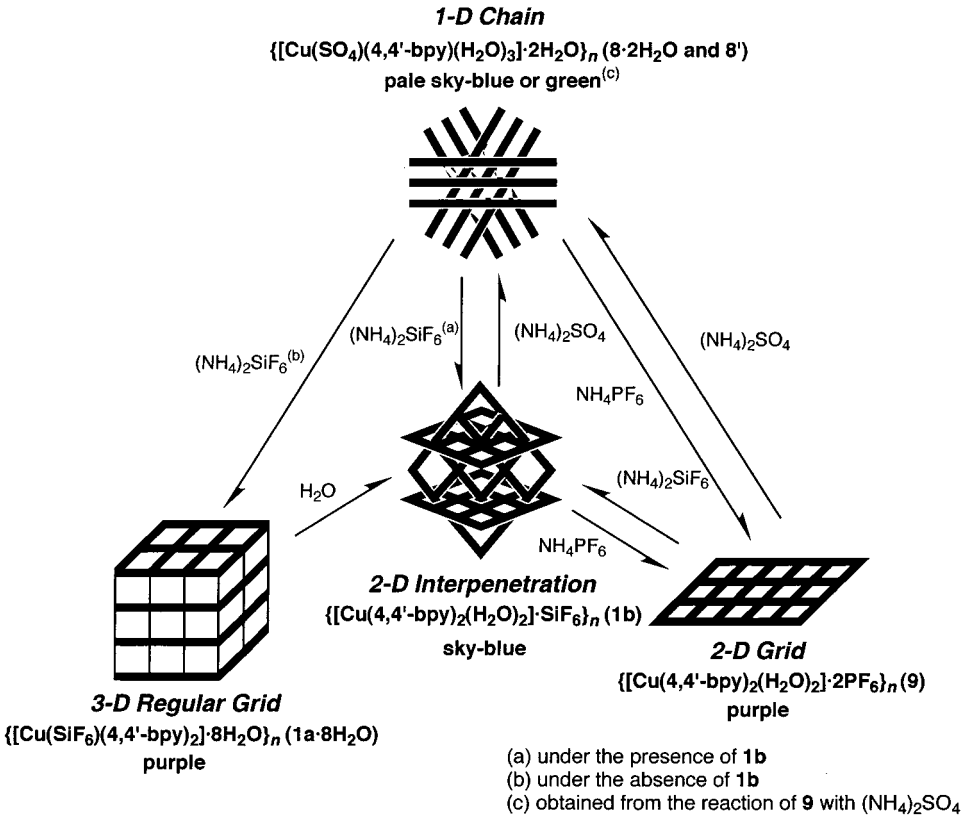

Several anion-exchangeable porous coordination polymers have so far been reported,[32−35] in which the microporous frameworks are maintained during the anion-exchange, thus called the second generation compounds. The anion-exchange properties of **1b** and **2b** were investigated, illustrating the third generation system.[7]

Microcrystals of **1b** were immersed in a $(NH_4)_2GeF_6$ (excess) solution for a few days. Although the color of the compound remained unchanged, the IR spectrum clearly shows a decrease in the intensity of the SiF_6^{2-} bands (748 and 480 cm^{-1}) and an increase in the intensity of a GeF_6^{2-} band (561 cm^{-1}), indicating that the compound has partially undergone the anion-exchange.[89] This compound maintains crystallinity during the anion-exchange process as illustrated by sharp peaks observed in the XRPD pattern, which is in a good agreement with that of a original sample **1b** as shown in Figure 9. The complete exchange of the counteranion is not attained. This is possibly because the GeF_6^{2-} anion is larger than SiF_6^{2-} and is readily trapped in the channel near the surface by hydrogen bond. Therefore, interpenetration into a deeper region of the anion is prevented. Indeed, no anion-exchange from GeF_6^{2-} to SiF_6^{2-} occurred in **2b**.

On the other hand, intriguing phenomena were observed in the case of SO_4^{2-} or PF_6^- anions. When the SO_4^{2-} dianion was employed for microcrystals of **1b**, the color changed from sky-blue to pale sky-blue. The phenomenon was monitored by EA, IR, and XRPD measurements. The compound appears to maintain crystallinity during the anion-exchange process as illustrated by sharp peaks in the XRPD pattern, but the peak pattern is different from that of the initial sample of **1b**. This is well demonstrated in Figure 10a and b, indicating that the initial compound is transformed to a new type of network including SO_4^{2-} instead of SiF_6^{2-}. Surprisingly, the XRPD pattern of the resultant compound is quite similar to that of 1-D polymer $\{[Cu(SO_4)(4,4'\text{-bpy})(H_2O)_3]\cdot 2H_2O\}_n$ (**8**·$2H_2O$) reported previously.[62] This is shown in Figure 10b and c. **8**·$2H_2O$ affords linear 1-D chain structures of $[Cu(SO_4)(4,4'\text{-bpy})(H_2O)_3]_n$, which form layers parallel to the *ab*-plane and stacking along the *c*-axis. Adjacent layers are rotated by 60° to produce triangle cavities with dimensions of ca. 3 Å. The SO_4^{2-} dianions, which weakly interact with Cu(II) ions, and free H_2O molecules occupy these triangle channels. The elemental analysis indicates that the ratio of starting **1b** and resultant **8**·$2H_2O$ is ca. 3:7.[90] The complete conversion under the condition was not attained. Furthermore, when the mixture was immersed in a H_2O solution containing 4,4′-bpy and an excess amount of $(NH_4)_2SiF_6$, microcrystals of only **1b** came back as illustrated in Figure 10d.

Interestingly, when the pure sample of **8**·$2H_2O$ was immersed in a H_2O solution containing 4,4′-bpy and an excess amount of $(NH_4)_2SiF_6$, the color immediately changed from pale sky-blue to purple, indicative of the quick transformation to the 3-D network **1a**·$8H_2O$. The IR data reveal that the position of a SiF_6^{2-} band (741 cm^{-1}) is similar to that of **1a**·$8H_2O$, and the XRPD pattern of the resultant compound is in good agreement with that of **1a**·$8H_2O$ as shown in Figure 11c. This result is apparently different from that of the mixed compounds of **1b** and **8**·$2H_2O$. Further stirring of this suspension causes a conversion of the 3-D network of **1a**·$8H_2O$ into the 2-D interpenetrated network of **1b**. A similar phenomenon was observed by using the $(NH_4)_2GeF_6$ dianion instead of the $(NH_4)_2$-

(89) Anal. Calcd for $\{[Cu(4,4'\text{-bpy})_2(H_2O)_2]\cdot 0.2SiF_6\cdot 0.8GeF_6\cdot 0.6H_2O\}_n$: C, 40.01; H, 3.56; N, 9.33. Found: C, 39.85; H, 3.63; N, 9.36.

(90) Anal. Calcd for $(\mathbf{1b})_{0.28}(\mathbf{8}\cdot 2H_2O)_{0.72}$: C, 34.37; H, 4.18; N, 8.02. Found: C, 34.21; H, 3.74; N, 8.06.

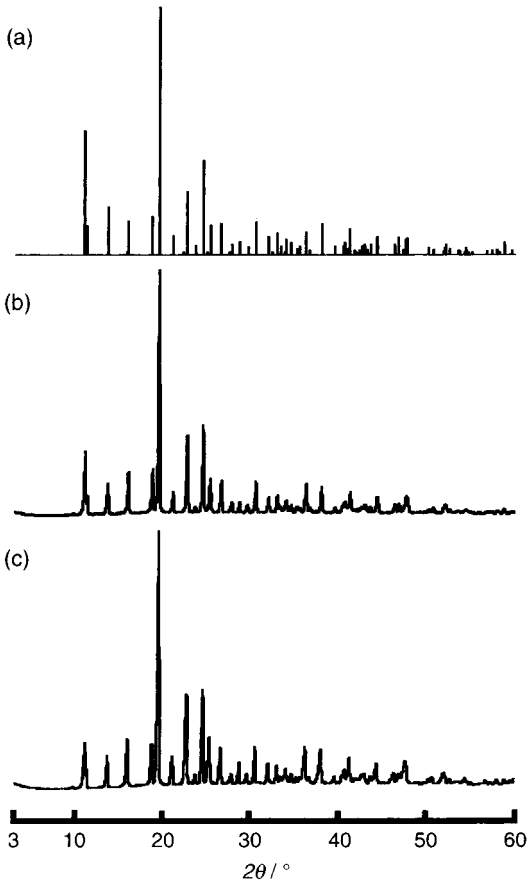

Figure 9. XRPD patterns of **1b** ((a) simulation and (b) observed patterns) and (c) solid obtained by immersing **1b** in a H_2O solution containing an excess amount of $(NH_4)_2GeF_6$.

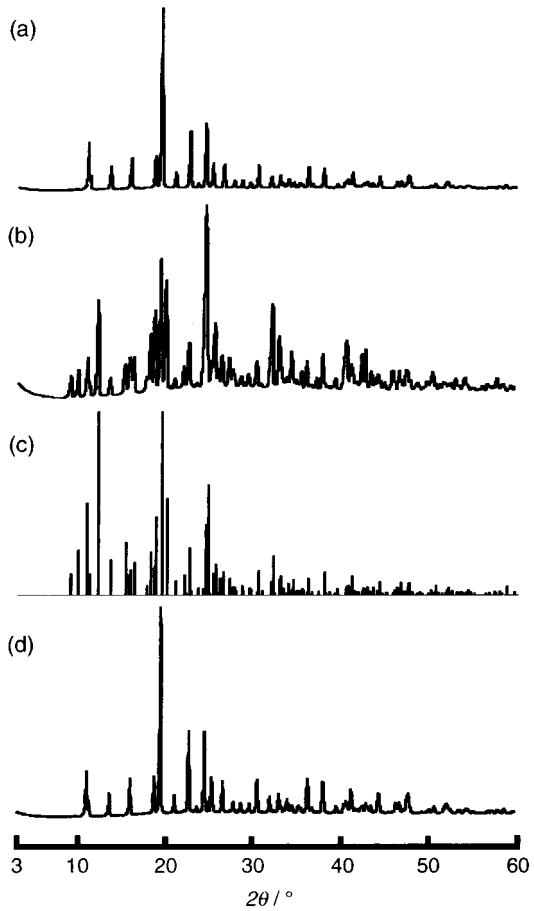

Figure 10. XRPD patterns of (a) **1b**, (b) solid obtained by immersing **1b** in a H_2O solution containing an excess amount of $(NH_4)_2SO_4$, (c) superposition of **1b** and **8**·$2H_2O$ (simulation patterns), and (d) solid obtained by immersing the partially exchanged sample in a H_2O solution containing the 4,4′-bpy ligand and excess amount of $(NH_4)_2SiF_6$.

SiF_6 dianion.[91] On the basis of this, the structural transformation from **8**·$2H_2O$ to **1a**·$8H_2O$ (or **2a**·$8H_2O$) first occurs, then finally **1b** (or **2b**) is completed by use of the SO_4/SiF_6 anion system.

It is worth noting that the PF_6^- anion also promotes a framework transformation, whose phenomenon was monitored by EA, IR, and XRPD measurements (see Experimental Section). In Scheme 4, the treatment of **1b** with NH_4PF_6 solution affords $\{[Cu(4,4'\text{-bpy})_2(H_2O)_2]\cdot 2PF_6\}_n$ (**9**), clearly showing the disappearance of intense SiF_6^{2-} bands (748 and 480 cm^{-1}) of **1b** and the appearance of an equally intense PF_6^- band (843 cm^{-1}). Concomitantly, the color of the compound turned from sky-blue to purple. Compound **9** represents an XRPD pattern with rather broad peaks, clearly different from the original pattern as illustrated in Figure 12a and b. The 2-D interpenetrated framework of **1b** was well reproduced by immersing **9** in aqueous solution with an excess amount of $(NH_4)_2SiF_6$ (Figure 12c). In this sense, the transformation is reversible.

A reversible transformation between **8**·$2H_2O$ and **9**, accompanying the anion exchange, was also observed. When the pure sample of **8**·$2H_2O$ was immersed in a H_2O solution with the 4,4′-bpy ligand and an excess amount of NH_4PF_6, the compound **9** was obtained. In contrast, when **9** was immersed in a H_2O solution with an excess amount of $(NH_4)_2SO_4$, the resultant solid, **8′**, was green and different from **8**·$2H_2O$ (pale sky-blue). The IR measurement of **8′** shows the disappearance of the intense PF_6^- band (843 cm^{-1}) and the appearance of an equally intense SO_4^{2-} band (1107 cm^{-1}). The EA and XRPD measurements reveal that the structure of **8′** is quite similar to that of **8**·$2H_2O$, representing a 1-D chain structure. Compound **9** formed again when **8′** was immersed in a H_2O solution with the 4,4′-bpy ligand and an excess amount of NH_4PF_6. The difference of the color in **8**·$2H_2O$ and **8′** is probably due to the difference in strength of the Cu−O (SO_4) bond. Each Cu(II) ion in **8**·$2H_2O$ has a distorted octahedral environment with two nitrogen atoms of 4,4′-bpy ligands (2.044 and 2.049 Å) and two oxygen atoms of H_2O molecules (1.952 and 1.976 Å) in the basal plane and one oxygen atom of a H_2O molecule (2.207 Å) and one oxygen atom of a SO_4^{2-} dianion (2.673 Å) in the axial sites. The UV−vis spectra show that the d−d transition of the Cu(II) ion in **8′** (green) appears at a higher energy (703 nm) than that of **8**·$2H_2O$ (sky-blue) (712 nm), associated with the different mode in coordination of SO_4^{2-} between **8′** and **8**·$2H_2O$.

However, when **2b** was immersed in aqueous solution in the presence of an excess amount of $(NH_4)_2SiF_6$, NH_4PF_6, or $(NH_4)_2SO_4$, no anion-exchange occurred. This is associated with the size of GeF_6^{2-} anions; the anion is too large to go through the small channel windows (ca. 2 × 2 $Å^2$).

The reversible structural conversions induced by anions in this manuscript are unique and useful for framework design.

(91) The partially exchanged compound $(\mathbf{2b})_x(\mathbf{8}\cdot 2H_2O)_{1-x}$ was not obtained from the reaction of **2b** with an excess amount of $(NH_4)_2SO_4$. Therefore, we prepared the partially exchanged compound artificially (the molar ratio, **2b**:**8**·$2H_2O$ = 3:7).

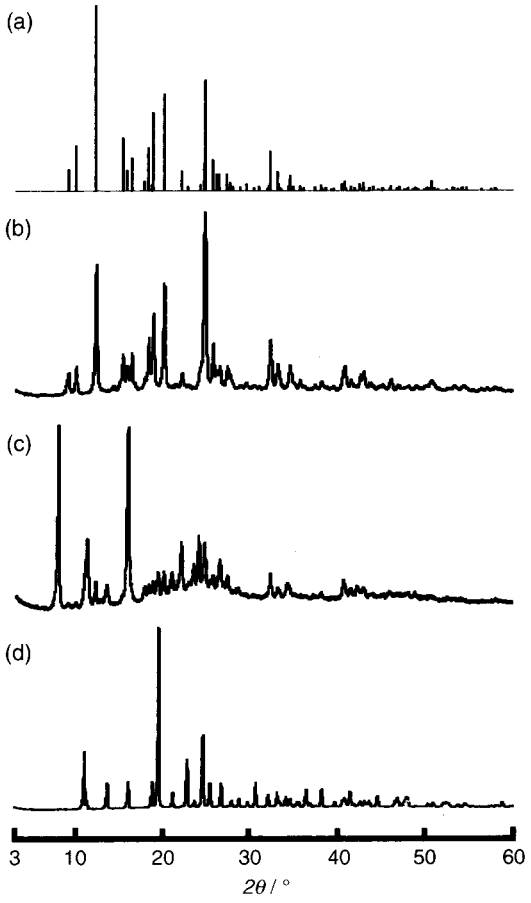

Figure 11. XRPD patterns of pure **8**·2H_2O ((a) simulation and (b) observed patterns), (c) purple solid immediately obtained by immersing pure **8**·2H_2O in a H_2O solution containing the 4,4′-bpy ligand and excess amount of $(NH_4)_2SiF_6$, and (d) sky-blue solid obtained by long immersing pure **8**·2H_2O in a H_2O solution containing the 4,4′-bpy ligand and an excess amount of $(NH_4)_2SiF_6$.

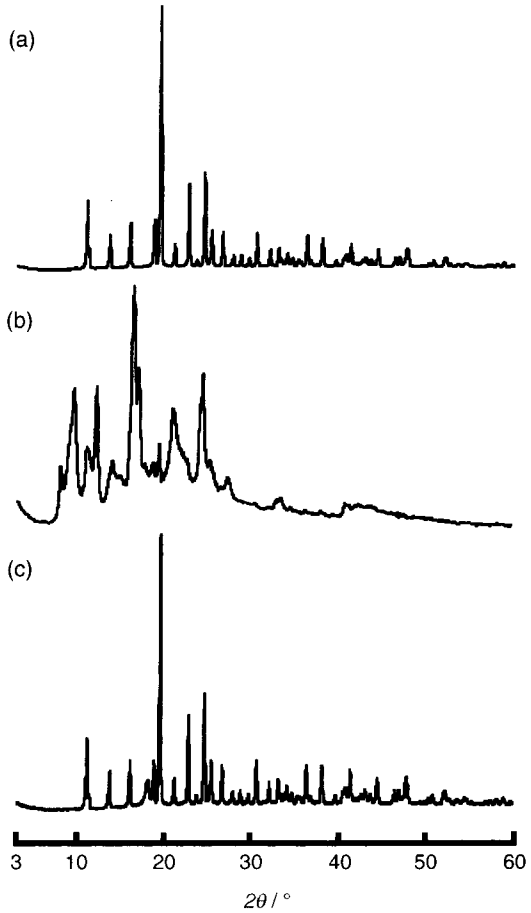

Figure 12. XRPD patterns of (a) **1b**, (b) solid obtained by immersing **1b** in a H_2O solution containing an excess amount of NH_4PF_6, and (c) solid obtained by immersing the exchanged sample in a H_2O solution containing an excess amount of $(NH_4)_2SiF_6$.

Recently, one example has been reported,[52] in which the structural conversions happen by slight movement of CN substituent groups of the ligand. In contrast, the anion-exchange in this work shows drastic reversible structural transformations among the 3-D network **1a**·8H_2O, the 2-D interpenetrated framework **1b**, the 1-D chain **8**·2H_2O and **8′**, and the 2-D noninterpenetrated framework **9**, with Cu−N (4,4′-bpy) bond formation and cleavage. These four types of complexes incorporate the anions in different modes as shown in Scheme 5. The SiF_6^{2-} dianions in **1a**·8H_2O become incorporated between the Cu(II) centers by coordination bonds, while the SiF_6^{2-} dianions in **1b** are not coordinated to the Cu(II) ions but are linked with coordinated H_2O molecules by hydrogen bonds. The SO_4^{2-} dianions in **8**·2H_2O and **8′** are ligated to the Cu(II) ions by coordination bonds in the monodentate fashion. The PF_6^- anions in **9** are probably coordination-free, because each Cu(II) center is coordinatively saturated by four nitrogen atoms of 4,4′-bpy ligands and two oxygen atoms of H_2O molecules. Furthermore, it is worth noting that these Cu-4,4′-bpy polymers can incorporate counteranions (AF_6^{2-} (A = Si, Ge), PF_6^-, and SO_4^{2-}) with various sizes and charges by changing the overall structures; in a sense, we can regard this as an anion receptor having flexible Cu(II)-4,4′-bpy frameworks. These results also reveal that the structures in the Cu(II)-4,4′-bpy system considerably depend on counteranions, which are, therefore, regarded as the framework-regulator.

In the anion-exchange process observed in this manuscript, not only the micropore width and shape but also the electrostatic affinity between Cu(II) ions and counteranions are important factors governing the drastic structural transformation. In addition, the competition for the Cu(II) sites between counteranions and coordinated guest molecules (H_2O molecule in this case) makes the behavior of the anion-exchange fruitful.

Conclusions

On the basis of a combination of Cu(II) ion and 4,4′-bpy, a variety of coordination polymer frameworks were created by using the framework-regulator AF_6 anions. The obtained frameworks are *3-D Regular Grid* (**1a**·8H_2O and **2a**·8H_2O), *2-D Interpenetration* (**1b** and **2b**), *2-D Double-Layer* (**3**·2H_2O·4EtOH and **4**·2H_2O·4EtOH), *3-D Undulated Grid* (**5**·2PF_6·2H_2O), and *2-D Grid* (**6**·2MeCN and **7**). The 3-D porous coordination polymers, **1a**·8H_2O, **2a**·8H_2O, and **5**·2PF_6·2H_2O, afford rigid microporous channels with dimensions of ca. 8 × 8 Å^2 and 6 × 2 Å^2 for **1a**·8H_2O and **2a**·8H_2O, and ca. 4 × 3 Å^2 and 3 × 3 Å^2 for **5**·2PF_6·2H_2O. These compounds show the high adsorption ability for the methane gas (second generation compounds), illustrating that the van der Waals mechanism operates well in the case of microporous coordination polymers. It is worth noting that the selection of AF_6 anions as the

Scheme 5

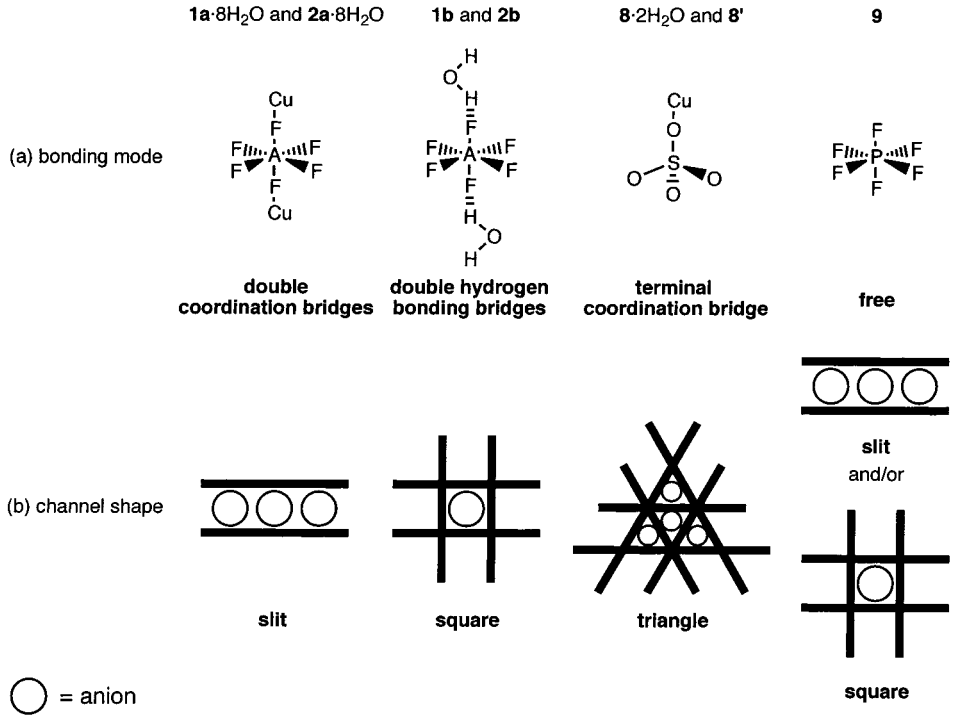

framework-regulator in the Cu(II)/4,4′-bpy system is of significance for the construction of 3-D porous networks. Interestingly, the 3-D networks **1a**·$8H_2O$ and **2a**·$8H_2O$ suitable for gas adsorption (second generation compounds) are transformed into the 2-D interpenetrated networks **1b** and **2b** suitable for the anion-exchange in the presence of H_2O (third generation compounds). This 2-D interpenetrated network **1b** shows unprecedented unique anion-exchange properties, in which the drastic structural conversion in the process of the anion-exchange occurs. This finding contains a basic concept for an anion sensor based on spectroscopic properties, characteristic of color change, and implies that the 4,4′-bpy-bridged porous coordination polymers are suitable for the construction of not only the second generation compounds but also the third generation compounds. When PF_6^- as the framework-regulator is employed with coexistent anions, various types of porous coordination networks depending on coexistent anions (ClO_4^-, BF_4^-, NO_3^-, and SO_4^{2-}) were obtained as shown in Scheme 2, in which novel types of frameworks with mixed anions have been created (**4**·$2H_2O$·4EtOH, **5**·$2PF_6$·$2H_2O$, and **7**). In particular, **5**·$2PF_6$·$2H_2O$ has a rare mixed-pillar structure. All the structures strongly depend on counteranions with the aid of guest solvents.

Acknowledgment. This work was supported by a Grant-in-Aid for Scientific Research from the Japanese Ministry of Education, Science, Sports, and Culture, Japan. The authors are most grateful to Mr. Kenji Seki (Osaka Gas Company, Ltd.) for the measurements of the adsorption of methane and argon gases. The authors also acknowledge Dr. Tatsuo Wada and Miss Kimiko Kobayashi (The Institute of Physical and Chemical Research (RIKEN)) for the measurements of the X-ray single-crystal diffraction data.

Supporting Information Available: Figures S1−S9, representing TGA data, XRPD data, and HK differential pore volume plot, and Tables S1−S35, listing full crystallographic details, fractional atomic coordinates, anisotropic displacement parameters, bond distances and angles, and hydrogen atom positions (PDF). An X-ray crystallographic file (CIF). This material is available free of charge via the Internet at http://pubs.acs.org.

JA0113192